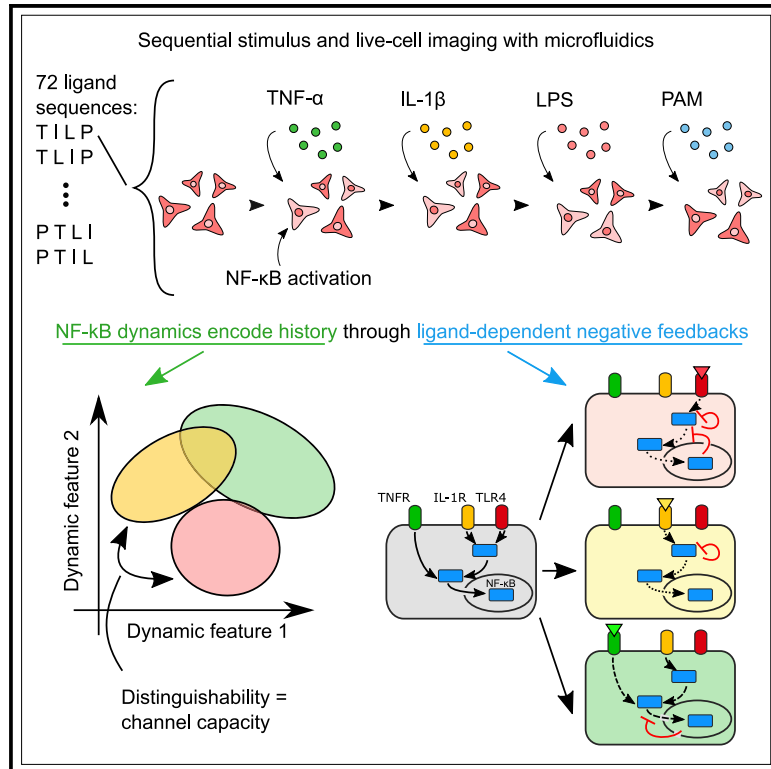


NF-κB memory coordinates transcriptional responses to dynamic inflammatory stimuli

Graphical abstract



Authors

Andrew G. Wang, Minjun Son,
 Emma Kenna, Nicholas Thom, Savaş Tay

Correspondence

tays@uchicago.edu

In brief

Wang et al. use microfluidic live-cell imaging to profile single-cell NF-κB responses to sequential stimulus with inflammatory ligands. NF-κB dynamics reflect ligand-dependent attenuation of subsequent signaling responses. These dynamics encode information about prior stimulus history and result from ligand-dependent induction of distinct negative feedbacks, which produce short-term memory.

Highlights

- Sequential inflammatory stimuli broadly result in NF-κB response attenuation
- Variable attenuation of NF-κB dynamics encode information on prior stimulus history
- Transcriptomics and mathematical modeling reveal ligand-dependent negative feedback
- Induced negative feedbacks alter subsequent signaling to produce short-term memory



Article

NF- κ B memory coordinates transcriptional responses to dynamic inflammatory stimuli

Andrew G. Wang,^{1,2,3} Minjun Son,^{1,3} Emma Kenna,¹ Nicholas Thom,¹ and Savaş Tay^{1,4,*}¹Pritzker School of Molecular Engineering, University of Chicago, Chicago, IL 60637, USA²Medical Scientist Training Program, University of Chicago, Chicago, IL 60637, USA³These authors contributed equally⁴Lead contact*Correspondence: tays@uchicago.edu<https://doi.org/10.1016/j.celrep.2022.111159>**SUMMARY**

Many scenarios in cellular communication require cells to interpret multiple dynamic signals. It is unclear how exposure to inflammatory stimuli alters transcriptional responses to subsequent stimulus. Using high-throughput microfluidic live-cell analysis, we systematically profile the NF- κ B response to different signal sequences in single cells. We find that NF- κ B dynamics store the short-term history of received signals: depending on the prior pathogenic or cytokine signal, the NF- κ B response to subsequent stimuli varies from no response to full activation. Using information theory, we reveal that these stimulus-dependent changes in the NF- κ B response encode and reflect information about the identity and dose of the prior stimulus. Small-molecule inhibition, computational modeling, and gene expression profiling show that this encoding is driven by stimulus-dependent engagement of negative feedback modules. These results provide a model for how signal transduction networks process sequences of inflammatory stimuli to coordinate cellular responses in complex dynamic environments.

INTRODUCTION

Exposure to pathogenic stimuli results in acute secretion of inflammatory cytokines, followed by a gradual rise and fall in anti-inflammatory cytokines and growth factors (Hackett et al., 2008; Kiers et al., 2017; Luan et al., 2019; Rao et al., 2010). The sequence (temporal ordering) of these stimuli provides information about the local tissue environment to nearby cells, and disruption of this progression is linked to pathology. For example, inflammatory signals in sepsis and chronic inflammation dramatically reshape the innate immune response to subsequent challenges (Deng et al., 2013; Foster et al., 2007; Heremans et al., 1990; Luan et al., 2019). Furthermore, efforts to engineer the inflammatory response in adjuvant therapy require understanding how prior exposure alters subsequent stimulus responses (Lérias et al., 2020; Pulendran et al., 2021).

Despite the diversity of inflammatory signals, many of these converge on few signaling networks with shared intracellular kinases and activated transcription factors. Pathogenic ligands which activate the Toll-like receptor (TLR) family and pro-inflammatory cytokines secreted by host sentinel cells all converge on a small set of key inflammatory transcription factors, including the canonical NF- κ B family transcription factor RelA (Hayden and Ghosh, 2012; Kawasaki and Kawai, 2014; Wajant and Scheurich, 2011). Patterns of NF- κ B activation over time, or activation dynamics, transmit information about stimulus identity and coordinate the subsequent inflammatory response. Ligands induce distinct dynamics of NF- κ B nuclear translocation, which

facilitate accurate information transmission from extracellular signals to expression of response genes (Adelaja et al., 2021; Kellogg et al., 2017). NF- κ B dynamics reshape the accessible chromatin landscape of the cell and regulate gene expression induced by each stimulus (Cheng et al., 2021; Sen et al., 2020). However, it is unknown how prior signal exposure alters NF- κ B dynamics. If prior stimuli induce distinct feedback responses which modulate a signaling network, it raises the possibility that activation dynamics can encode information about both the cell's current stimulus and prior history.

Previous studies of innate immune signaling focused on population-level effects of stimulus history at timescales of days to weeks (Divangahi et al., 2021; Foster et al., 2007; Luan et al., 2019; Novakovic et al., 2016). These studies report that innate immune memory can induce both priming, where response to subsequent stimulus is stronger (Deng et al., 2013; Novakovic et al., 2016), and tolerance, where the subsequent response becomes attenuated (Butcher et al., 2018; Foster et al., 2007; Ifrim et al., 2014). However, innate immune memory at short timescales is poorly studied due to the difficulties in strict control of stimulus timing and continual cell monitoring. Furthermore, population averaged readouts often blur single-cell dynamics and may not represent the actual cellular response.

Here, we explored how prior stimulus history alters subsequent signaling responses in the NF- κ B signaling network by combining automated microfluidic stimulation with live-cell imaging (Figure 1A). We found that prior stimuli produced distinct



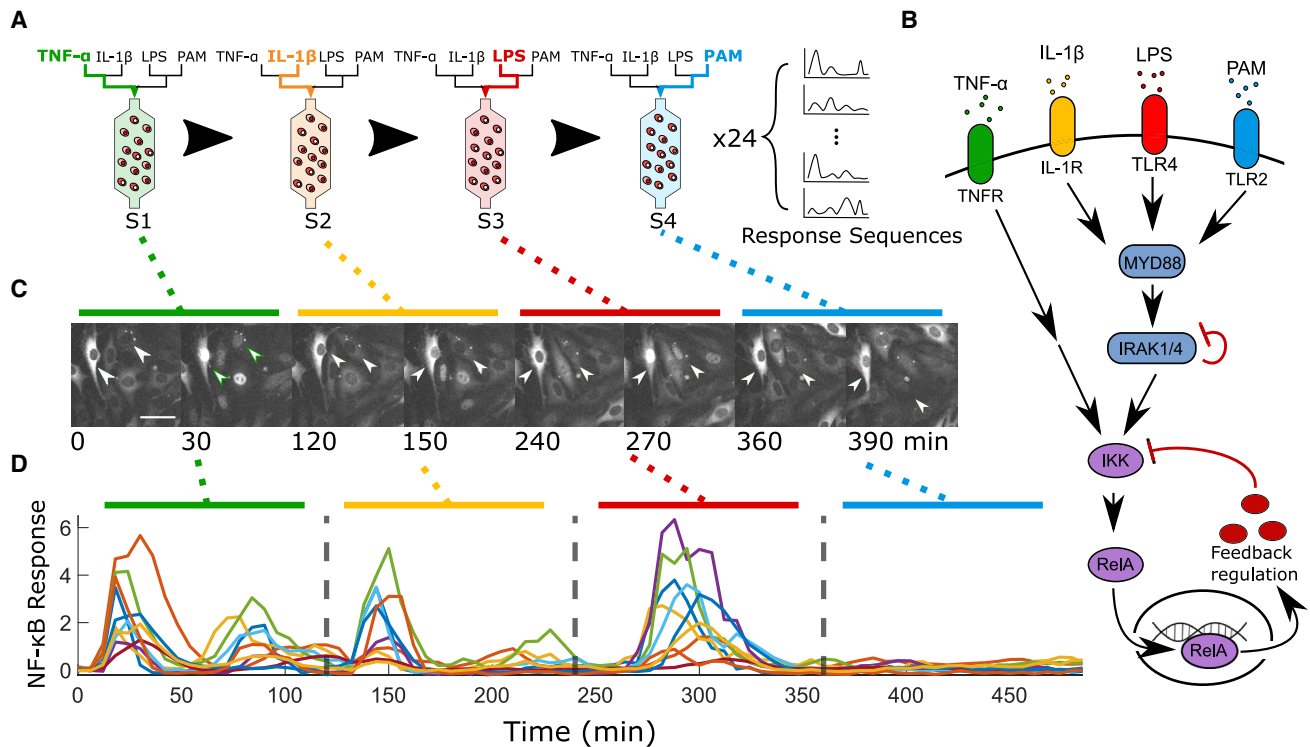


Figure 1. Microfluidic live-cell imaging tracks single-cell NF- κ B responses through multiple sequential stimuli

(A) Schematic representation of experimental conditions and microfluidic imaging setup. RelA-DsRed-tagged 3T3s were stimulated with non-repeating combinations of four ligands with in an automated microfluidic cell culture device.

(B) Schematic representation of TNF- α (TNFR), IL-1 β (IL-1R), LPS (TLR4), and PAM (TLR2) signaling converging on activation of RelA.

(C) Representative grayscale images of RelA nuclear translocation during stimulation with mid-dose TNF- α (0 min), IL-1 β (120 min), LPS (240 min), and PAM (360 min). RelA nuclear translocation in single cells (white arrows) is shown. Scale bar, 50 μ m.

(D) Quantification of nuclear/cytoplasmic NF- κ B over imaging interval. Gray dashed lines indicate when new stimulus was provided. See also *Videos S1* and *S2*.

attenuation patterns in subsequent NF- κ B signaling dynamics through differential regulation of negative feedbacks. These patterns encode information about the cell's prior history, showing that the NF- κ B network stores information about the temporal sequence of environmental signals and transmits that information in the inflammatory response.

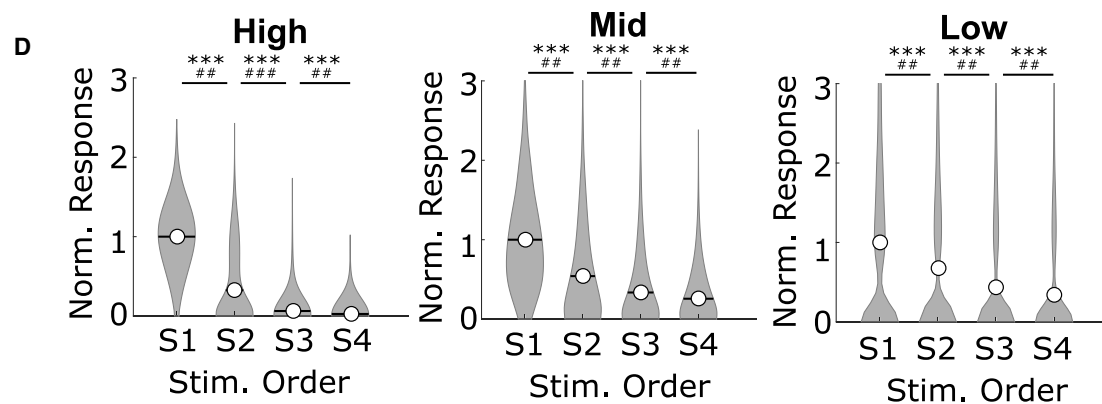
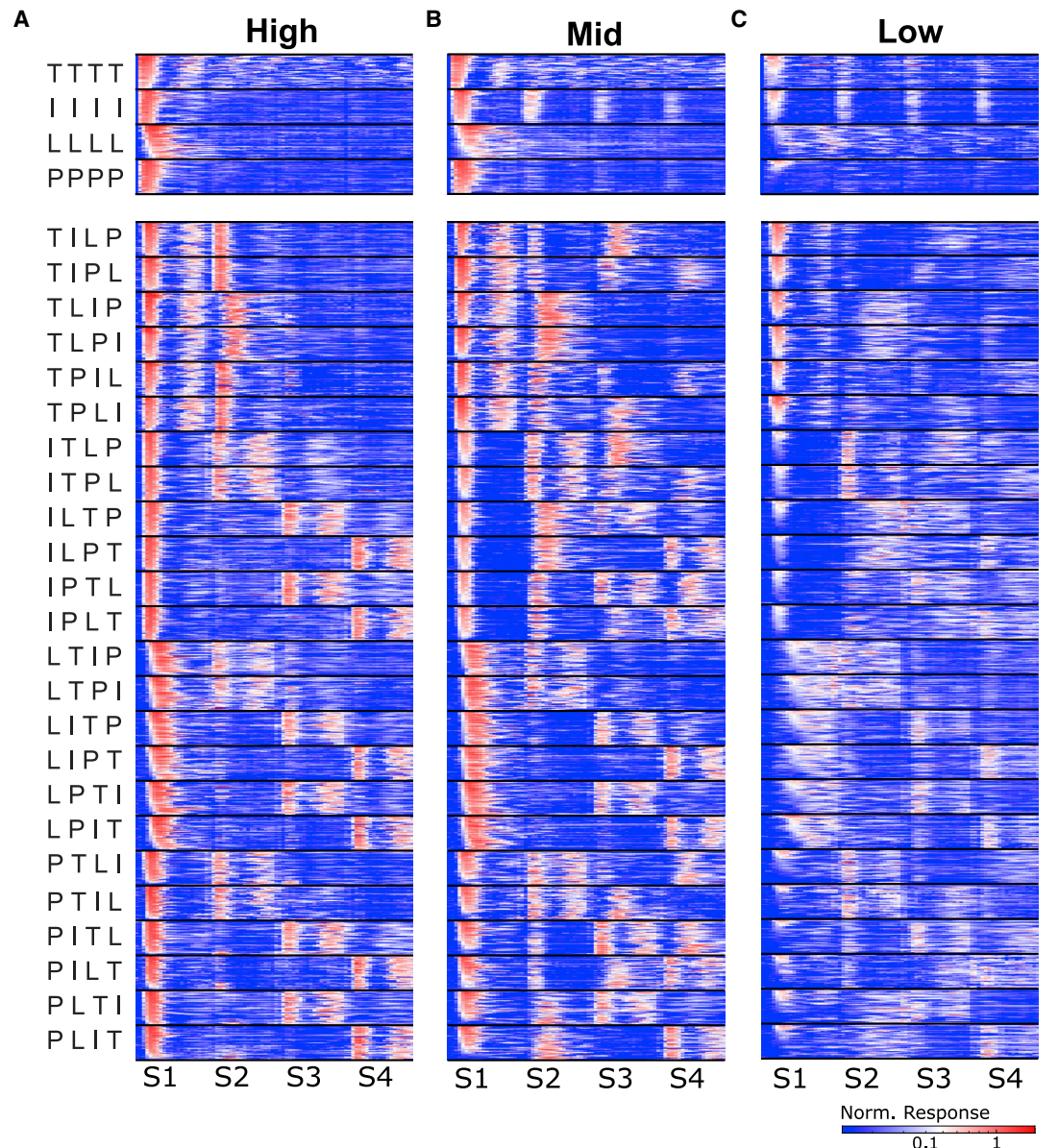
RESULTS

Prior ligand history influences NF- κ B activation to subsequent stimuli

We focused on the interactions between four inflammatory ligands, tumor necrosis factor alpha (TNF- α), interleukin-1 β (IL-1 β), lipopolysaccharide (LPS), and PAM2CSK4 (PAM). TNF- α and IL-1 β are key pro-inflammatory cytokines that are secreted by sentinel cells and which activate TNFR and IL-1R, respectively (Lawrence, 2009). LPS is a cell wall component of Gram-negative bacteria that activates TLR4, while PAM is a synthetic analog of bacterial lipopeptides that activates TLR2/6 (Kawasaki and Kawai, 2014). Thus, LPS and PAM represent pathogen signals, which would trigger local secretion of TNF- α and IL-1 β in an infection scenario. Signaling for LPS, PAM, and IL-1 β share the receptor-associated adaptor protein MyD88 and downstream components, including IRAK1 (Figure 1B) (Cohen, 2014). In

contrast, TNF- α signaling acts through a different set of receptor-associated intermediaries (Hayden and Ghosh, 2012). All these pathways converge at activation of I κ B kinase (IKK), which mediates nuclear translocation of RelA (Hayden and Ghosh, 2012; Kawasaki and Kawai, 2014). Multiple levels of negative feedback regulate this network, including auto-inhibitory phosphorylation of IRAK1 and several transcriptionally regulated negative feedback proteins, such as A20 and I κ B ϵ (Figure 1B) (Adamson et al., 2016; DeFelice et al., 2019; Kearns et al., 2006; Shembade et al., 2010; Son et al., 2021). Each of these negative feedback proteins targets different components in the NF- κ B signaling network (Figure 1B) (DeFelice et al., 2019).

To characterize how prior histories shape the NF- κ B response to a subsequent ligand, we used a microfluidic platform to provide sequential stimuli to RelA^{-/-} NIH/3T3 fibroblasts (3T3s) expressing a RelA-DsRed fusion protein (Figure 1A) (Kellogg et al., 2014; Son et al., 2021). By continuously imaging 3T3s in this platform, we evaluated NF- κ B dynamics under a series of stimuli without disrupting the cells (Figures 1C and 1D; Videos S1 and S2). To establish a baseline for comparison between the history of the same and different ligands, we stimulated cells with the same ligand four times. In general, prior stimulus with a ligand weakened subsequent responses to the same ligand, which is consistent with previous work with repeated ligand stimulus



(legend on next page)

(Adamson et al., 2016; Ashall et al., 2009; Son et al., 2021). LPS and PAM only produced a response after the first stimulus, while TNF- α and IL-1 β exhibited weak responses after the second to fourth stimulus depending on dose (Figures 2A–2C). We then systematically profiled the effects of prior history by stimulating cells with non-repeating sequences of all four ligands. This approach produced 24 unique stimulus conditions. The first stimulus (S1) is provided to cells without prior inflammatory ligand exposure, and thus induces a “naive” response. However, the second, third, and fourth stimuli (S2–S4) would induce NF- κ B responses affected by one, two, or three prior ligands, respectively. We used the response to a particular ligand at S1 as a baseline for comparing how different prior stimulus sequences change the response to that ligand. In addition, to test how stimulus dose changes prior history effects, we calibrated high, mid, and low doses for each ligand based on the percentage of activated cells (Figures S1A–S1E), then repeated the 24 stimulus sequences for each dose. In our initial dataset of 72 conditions, we analyzed more than 10,000 single cells (Figures 2A–2C and S1F–S3) with a range of prior histories and stimulus doses.

To observe general trends in ligand response, we first examined how the response to a specific ligand changed depending on its order in a stimulus sequence. All single-cell responses in each sequence position were grouped by ligand and normalized to the mean S1 response for that ligand (Figures 2A–2C and S4A–S4C). When we compared the amplitude changes over the four sequence positions, we observed that response for each ligand decreased from S1 to S4 (Figure 2D). Even in low-dose conditions, where response heterogeneity results in highly variable response amplitudes, ligand responses decreased from S1 to S4. Similar trends were observed when quantifying the area under the curve (AUC) of the response instead of the maximum response amplitude (Figure S4D). From these observations, we concluded that prior exposure history primarily attenuates signaling responses to subsequent ligands. However, we also noted that distinct patterns of attenuation existed depending on ligand identity and dose. Even at high dose, where attenuation was strongest, cells responded to TNF- α stimulus irrespective of prior history (Figures 2A and S4A). At mid and low dose, each ligand displayed different history responses. LPS and TNF- α responses exhibited the weakest attenuation, with some level of stimulus response retained across most conditions, while IL-1 β and PAM responses showed large variability in response depending on prior stimulus history (Figures 2B, 2C, S4B, and S4C). Thus, particular histories of ligand exposure can alter subsequent stimulus responses in a consistent and predictable manner.

The NF- κ B network reflects information about prior ligands in the subsequent response

If particular ligand histories alter subsequent response dynamics in a distinctive manner, it would be possible to characterize a cell’s prior history through its response to subsequent stimuli. However, the regulation of a genetic network is inherently noisy, resulting in diverse responses to identical stimulus at the single-cell level and over time (Elowitz et al., 2002; Newman et al., 2006; Taniguchi et al., 2010). This variability may impact how accurately individual cells can reflect prior history in subsequent responses. Thus, we needed to address single-cell variability in characterizing how effectively prior history is reflected in subsequent responses.

We used information theory to characterize the distinguishability of NF- κ B responses to different stimulus orders despite single-cell noise. In information theory, the maximum information transmittable by a noisy network is described by the channel capacity (CC) (Figure 3A). In our case, the CC represents the maximum distinguishability of groups in a population response. Therefore, the CC can be used to quantify the accuracy of signal transduction in the NF- κ B network (Adelaja et al., 2021; Cheong et al., 2011; Selimkhanov et al., 2014; Tudelska et al., 2017). We first measured the CC of the NF- κ B network in distinguishing all 24 stimulus conditions in each dose. If the NF- κ B network did not retain information about prior history, we would expect the CC to stay the same or decrease from S1 to S4, since the effect of noise is enhanced with signal attenuation (Figure 2D) (Simpson et al., 2009). However, we found that CC increased from S1 to S2 despite attenuation (Figure 3B). Even later in the stimulus sequence at S3 and S4, where attenuation became more pronounced, the CC still remained above the baseline at S1. These observations indicate that, even though the same four ligands are used for stimulation in each sequence, more distinguishable responses are present in S2–S4. Thus, the NF- κ B signaling network retains information about prior history and coordinates subsequent stimulus responses based on prior exposure.

To investigate how prior history affected the response for each ligand, we quantified the CC for each ligand at positions S1–S4. We grouped the samples based on ligand and sequence position and calculated the CC among the samples within each group (Figure 3C). Ligands unaffected by prior history would produce identical responses and a CC of zero, while ligands for which prior history changes activation dynamics would see an increase in CC at S2–S4. We found that the CC specific to each ligand generally rose at S2 and remained elevated at S3–S4. In other words, more distinct response behaviors are present in S2–S4, indicating that a cell’s response to a specific ligand is significantly changed based on the cell’s prior history. However,

Figure 2. Single-cell NF- κ B activation traces reveal ligand and dose-specific attenuation of signaling by prior stimuli

(A–C) NF- κ B response dynamics over 2 h of stimulus for each ligand. Fifty randomly selected single-cell traces from two independent replicates are displayed for each condition. Each row shows the nuclear NF- κ B level of a single-cell measured by time-lapse microscopy, and the x axis shows the time. Heatmap columns are arranged from the first stimulus (S1) to the fourth stimulus (S4). Stimulus orders are shown to the left of the first heatmap, where T stands for TNF- α , I for IL-1 β , L for LPS, and P for PAM. Heatmap for response to four consecutive feedings with the same ligand are shown above the combinatorial orders. Heatmap colors are normalized based on the high-dose S1 response to each ligand.

(D) Single-cell responses from S1 to S4, normalized to the mean of corresponding S1 response (>2,000 cells for each condition). Open circle and line show the mean. Bonferroni corrected Wilcoxon rank-sum test; ***p < 10⁻⁴. Fold change difference between sample means >1 (#), >1.25 (##), or >4 (###). See also Figures S1–S4.

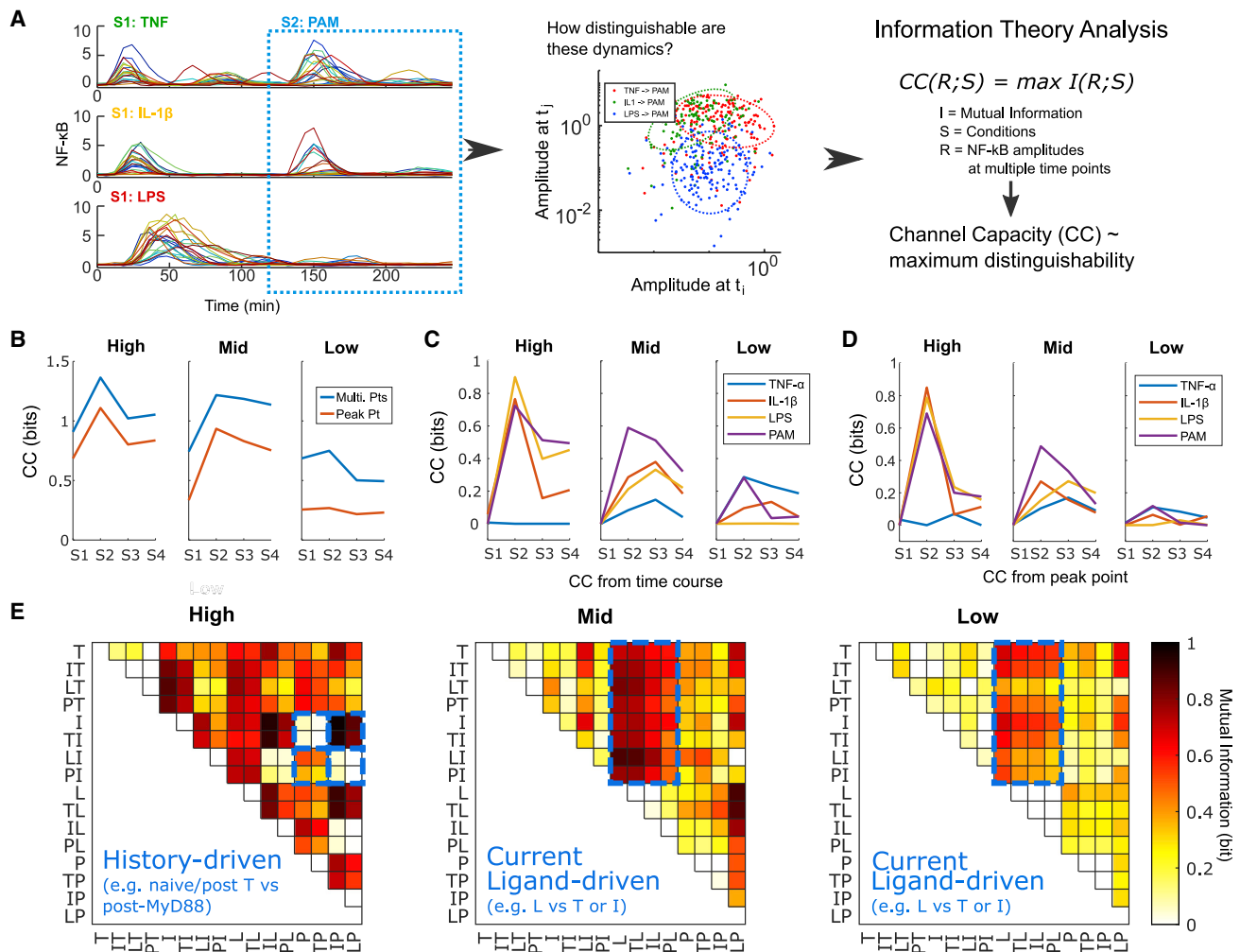


Figure 3. Information about prior stimulus history is reflected in the dynamics of subsequent NF-κB responses

(A) Schematic representation of information theory analysis. Nuclear NF-κB levels at six different time points (20, 30, 40, 50, 70, and 90 min) from multiple conditions are used as inputs to calculate the mutual information between conditions. Channel capacity (CC) represents the maximum mutual information between conditions.

(B) Distinguishability among all samples at S1–S4. CC is calculated from the six-dimension vector (blue line) and compared with the CC from a single feature (red line).

(C) CC among samples exposed to the indicated ligand at S1–S4 calculated using the six-dimension vector. CC in S2–S4 indicates how accurately the NF-κB network reflects the prior history in the response to the indicated ligand.

(D) As in (C), CC among all samples with the same ligand at each sequence interval but calculated using a single feature.

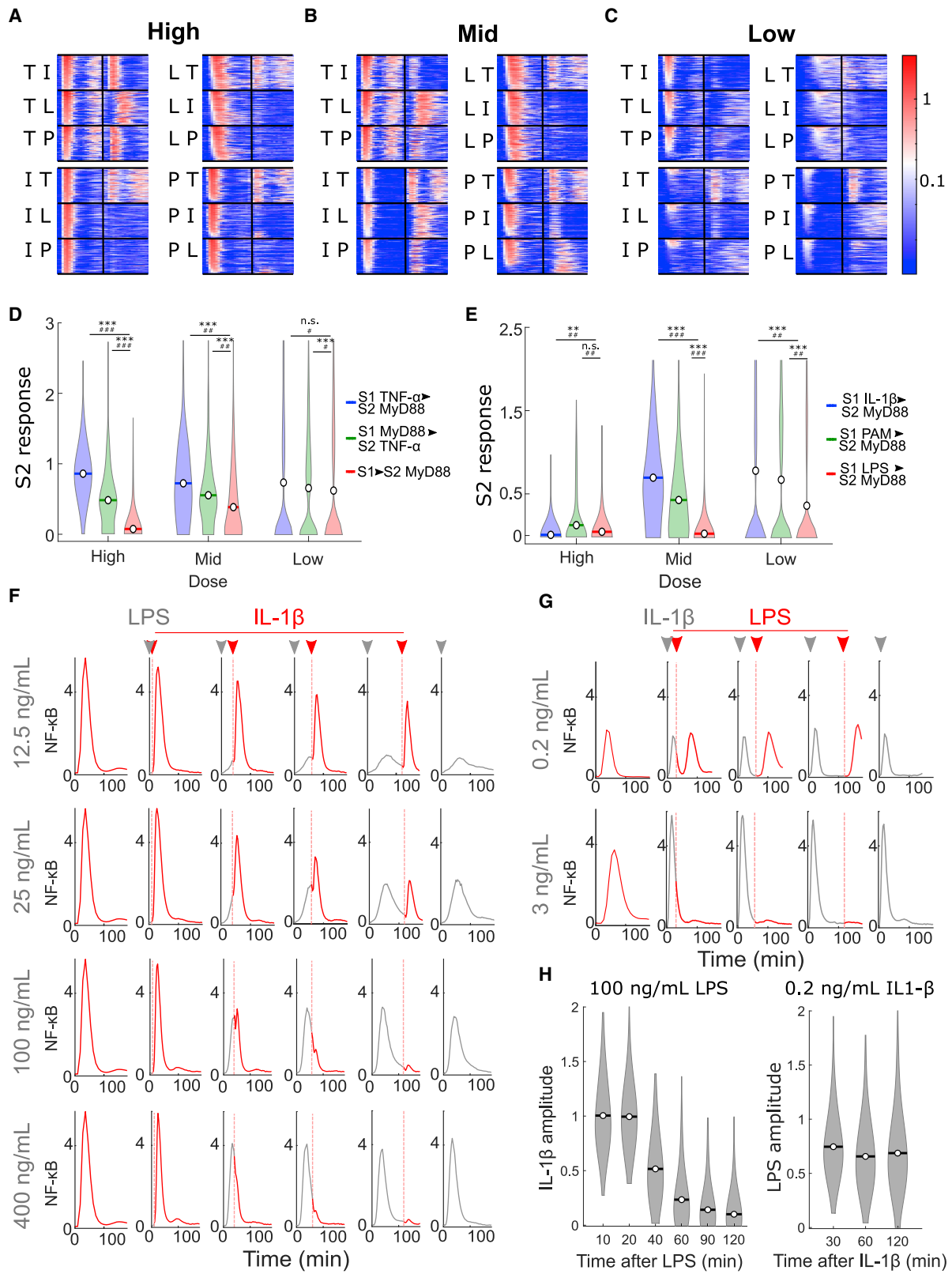
(E) Mutual information (MI) between ligand response dynamics (S1 and S2 only). T, I, L, and P indicate the order of the stimulus. MI of 1 indicates complete distinguishability between two conditions.

TNF-α at high dose and LPS at low dose gained little information from prior history, which reflected our observations that prior history only weakly attenuated signaling in those samples (Figures 2A, 2C, S4A, and S4C). Nonetheless, the general trend of increased CC at S2–S4 compared with S1 suggests that the NF-κB network encodes information about prior history in subsequent responses.

We also noted that the dynamics of the NF-κB response play a major role in accurate information transmission from prior history. When we compared the CC using response amplitudes at multiple time points with the CC using a single feature (the

response amplitude when the mean was at its peak), we found that the CC from a single feature (Figures 3B, red lines and 3D) are substantially lower than the CC from the dynamic measurement (Figure 3B, blue lines and 3C). This indicates that alteration of NF-κB activation dynamics plays a role in transmitting information about prior history (Selimkhanov et al., 2014).

We then investigated which ligand responses were most distinguishable from each other by calculating the mutual information between a pair of ligand responses. We focused on the naive responses to a ligand at S1 and following another ligand at S2, resulting in a comparison of 16 conditions for each dose



(legend on next page)

(Figure 3E). In the comparison matrix, mutual information patterns at low and mid dose were primarily driven by differences between TNF- α or IL-1 β response dynamics and LPS or PAM response dynamics (e.g., comparing TNF- α and LPS). However, response to IL-1 β or PAM following LPS (LI or LP) also were distinguishable from almost every other response at mid dose. At high dose, the pattern of mutual information changed such that all TNF- α responses became highly distinguishable from other samples. Likewise, the naive and TNF- α -exposed responses to IL-1 β , LPS, and PAM also became distinguishable from the same responses following either IL-1 β , LPS, or PAM (e.g., TI versus LI or TL versus IL). This shift in mutual information patterns between low, mid, and high doses suggests that fundamentally distinct mechanisms could potentially mediate the effects of prior history in these dose ranges. Overall, these mutual information analyses confirmed that the NF- κ B response is distinguished based on ligand sequence at the single-cell level.

Prior stimuli attenuate the subsequent NF- κ B response in a ligand- and dose-dependent manner

To study how information about prior history is stored in the NF- κ B network, we investigated how different stimuli produced different patterns of attenuation (Figure 1C). At all three dose ranges, TNF- α signaling was only weakly attenuated by prior stimulus, while the attenuation of LPS, PAM, and IL-1 β signaling varied depending on the dose and identity of the prior ligand (Figures 2A–2C and S4A–S4C). LPS, PAM, and IL-1 β signaling all utilize a MyD88-dependent signal transduction pathway, including the shared signaling intermediary IRAK1 (Figure 1B) (Kawasaki and Kawai, 2014). IRAK1 has been reported to regulate itself through auto-inhibitory phosphorylation, which limits subsequent activation of IRAK1 by other stimuli (DeFelice et al., 2019). Thus, we hypothesized that prior MyD88-dependent signaling attenuates subsequent signaling in the same pathway, but that TNF- α is independent from this inhibition.

To test this hypothesis, we focused on how a single prior ligand affects the following response, i.e., how the S1 ligand response changes the S2 ligand response (Figures 4A–4C). The LPS response was delayed as both an S1 ligand and an S2 ligand (Figures 4A–4C) despite sharing the same intracellular

molecular pathway as PAM and IL-1 β (Adelaja et al., 2021; Kellogg et al., 2017; Werner et al., 2005). This feature has been linked to ligand-specific control of IKK activation dynamics, and has been proposed to be due to modulation of IKK cycling rates (Behar and Hoffmann, 2013; Werner et al., 2005). Indeed, we found that different IKK cycling rates could result in the delayed LPS response we observed experimentally (Figure S7E). We found that, following TNF- α stimulus, the response to MyD88-dependent ligands was weakly attenuated (Figure 4D, blue). Likewise, the response to TNF- α following MyD88-dependent stimuli was weakly attenuated (Figure 4D, green). In contrast, MyD88-dependent ligands attenuated subsequent signaling by other MyD88-dependent ligands in a dose-dependent manner (Figure 4D, red). At high and mid doses, exposure to MyD88-dependent ligands resulted in significantly attenuated signaling from other MyD88-dependent ligands compared with previous TNF- α exposure. Taken together, these results indicate that a prior history of TNF- α signaling minimally affected MyD88-dependent signaling and vice versa, while a prior history of MyD88-dependent signaling inhibited the response to other MyD88-dependent ligands in a dose-dependent manner.

If shared negative feedback is the primary cause of attenuation for subsequent MyD88-dependent signaling, each MyD88-dependent ligand should equally attenuate subsequent MyD88-dependent ligands. Although LPS is known to also utilize a MyD88-independent module mediated by TRIF and TRAM (Fitzgerald et al., 2003; Yamamoto et al., 2003), we found that the MyD88-independent pathway for LPS had minimal influence in these cells, as knocking out MyD88 was sufficient to abolish all response to LPS (Figures S5A–S5C). Thus, we expected LPS, PAM, and IL-1 β to equally inhibit the response to each other. At high dose, all three MyD88-dependent ligands indeed strongly attenuated subsequent responses (Figure 4E). In contrast, at mid and low doses, only LPS strongly attenuated subsequent MyD88-dependent signaling (Figure 4E, red), while IL-1 β and PAM allowed significantly stronger subsequent responses (Figure 4E, blue, green). Thus, at high dose, attenuation between LPS, PAM, and IL-1 β occurred symmetrically, while at mid and low doses, attenuation became asymmetric. Prior LPS stimulus inhibited subsequent IL-1 β /PAM response but not

Figure 4. Ligand- and dose-specific effects of prior history differentiate TNF- α from MyD88-dependent ligands and differentiate among MyD88-dependent ligands

(A–C) NF- κ B response dynamics over 2 h of stimulus for each ligand normalized to the mean amplitude of the naive (S1) high-dose response. Fifty single-cell traces randomly selected for each condition. All sequences of S1 and S2 ligands shown. All nine sequences shown at high (A), mid (B), and low (C) dose.
(D) Violin plot comparing the normalized S2 responses of the MyD88-dependent ligands (LPS, PAM, IL-1 β) following either TNF- α (blue) or another MyD88-dependent ligand (red) or the TNF- α response following a MyD88-dependent ligand (green) (>650 cells per condition). Open circles and lines show the mean.
(E) Violin plot comparing the normalized S2 MyD88-dependent responses following IL-1 β (blue), PAM (green), and LPS (red) stimulus at high, mid, and low doses (>340 cells per condition). Bonferroni corrected Wilcoxon rank-sum test; n.s. $p > 10^{-2}$, * $p < 10^{-2}$, ** $p < 10^{-3}$, *** $p < 1 \times 10^{-4}$. Fold change difference between sample means >1 (#), >1.25 (##), or >4 (###).
(F) Plot of mean trace for conditions where LPS is provided at 0 min (gray arrowhead) and switched to 3 ng/mL (high dose) IL-1 β after the indicated time (red arrowhead). Gray region and red regions of trace indicate NF- κ B response during LPS stimulus interval and after replacement with IL-1 β , respectively. Entirely red traces in the left column show an only IL-1 β response and entirely gray traces in the right column show an only LPS response. Each mean trace represents >100 single cells from 2 biological replicates.
(G) Plot of mean traces for conditions where 0.2 and 3 ng/mL (mid and high dose) IL-1 β are provided at 0 min and switched to 100 and 400 ng/mL (mid and high dose) LPS, respectively, after the indicated time. Gray region and red regions of trace indicate NF- κ B response during IL-1 β stimulus interval and after replacement with LPS, respectively. As in (F), entirely red traces in the left column show an only LPS response and entirely gray traces in the right column show an only IL-1 β response. Each mean trace represents >100 single cells over 2 biological replicates.
(H) Violin plot comparing the normalized response for 3 ng/mL IL-1 β following 100 ng/mL LPS or the response for 100 ng/mL LPS following 0.2 ng/mL IL-1 β . Each plot is derived from >100 cells per condition over 2 biological replicates. Open circles and lines show the mean. See also Figures S5, S6A, and S6B.

vice versa. Similarly, when we compared the JNK responses with MyD88-dependent ligands following either IL-1 β or LPS stimulus, we saw that symmetric attenuation took place at high dose but, at mid dose, only LPS maintained strong attenuation of MyD88-dependent JNK activation (Figures S5F–S5H). These data reproduced the asymmetry in attenuation observed in our NF- κ B measurements and suggest that asymmetric prior history effects may be broadly applicable in multiple inflammatory signaling pathways. Despite the highly shared pathways between LPS, PAM, and IL-1 β , prior LPS effects differ from prior PAM or IL-1 β effects in a dose-dependent manner.

Although our results suggest asymmetry in short-term history effects between MyD88-dependent ligands, innate immune signaling occurs on a range of timescales. Thus, we sought to understand the temporal range under which this asymmetry persists and extended the duration between S1 and S2 to 4, 6, and 8 h (Figures S5I–S5L). At these longer durations, we still observed similar ligand and dose-specific attenuations. TNF- α only weakly attenuated MyD88-dependent signaling through IL-1 β , while LPS and IL-1 β attenuated each other symmetrically at high dose. At mid dose, LPS still strongly attenuated IL-1 β , but not vice versa. At longer time intervals, both TNF- α -dependent attenuation of IL-1 β and IL-1 β -dependent attenuation of LPS strengthened, which suggests that longer duration stimuli may weaken the asymmetry between ligand histories. Nonetheless, the overall trends at increased duration were consistent with our findings after 2 h of stimulus, which indicates that these effects persist at longer durations.

Slow LPS-dependent negative feedback induces distinct attenuation in the subsequent stimulus response

While auto-inhibition of IRAK1 can explain symmetric attenuation at high ligand dose (DeFelice et al., 2019), as IRAK1 is shared by each of the MyD88-dependent ligands (Figure 1B), it could not explain our results at mid and low doses. Asymmetric cross-attenuation at mid and low doses suggests the existence of an additional negative feedback mechanism, which would be more strongly activated by LPS stimulation than by IL-1 β or PAM.

To study the characteristics of asymmetric attenuation of MyD88-dependent signaling, we examined how rapidly attenuation takes place upon stimulation with LPS. The timescale of attenuation can inform where in a signaling network the feedback acts. For example, rapid attenuation is unlikely to be driven by transcription and translation of downstream feedback genes. We stimulated cells with various doses of LPS (12.5–400 ng/mL), then stimulated the cells with high dose of IL-1 β (3 ng/mL) after 10–120 min of LPS stimulus (Figures 4F and S6A). Attenuation of IL-1 β signaling by high-dose LPS (400 ng/mL) was fast and strong, rapidly suppressing the subsequent IL-1 β response at all times except the shortest time interval (10 min). As IRAK1 is shared in the early part of the signaling pathway, this observation was consistent with rapid auto-inhibition of IRAK1. However, following lower doses of LPS, the IL-1 β response became gradually attenuated depending on duration of LPS stimulus (Figures 4F and 4H).

On the other hand, when we stimulated first with IL-1 β , then LPS, we did not observe gradual attenuation. Similar to high-

dose LPS, high-dose IL-1 β still produced immediate and strong attenuation of the LPS response, suggesting that auto-inhibition of IRAK1 still plays a major role in subsequent attenuation (Figures 4G and S6B). Increasing duration of stimulus with mid-dose IL-1 β , however, had no impact on attenuation of LPS signaling (Figure 4G). To compare the difference between prior stimulation with LPS and IL-1 β more clearly, we normalized the responses to the second stimulus to the corresponding naive responses (Figure 4H). As expected, the response to IL-1 β following LPS gradually decreased over time, while LPS response following IL-1 β remained consistent over time. These results suggest that an additional activation-time-dependent negative feedback process is differentially regulated by each MyD88-dependent ligand. This time dependence led us to hypothesize that this additional feedback response relies on NF- κ B-dependent gene expression.

Ligand-specific attenuation in MyD88-dependent signaling depends on activation of IKK

To test whether NF- κ B translocation and subsequent gene expression is necessary for asymmetric and ligand-dependent attenuation, we targeted the signaling intermediary IKK. IKK controls the activation and translocation of NF- κ B into the nucleus through degrading the inhibitory protein I κ B α (Figure 1B). Using PS1145, a reversible small-molecule inhibitor of the IKK- β subunit (Yamamoto et al., 2003; Yemelyanov et al., 2006), we blocked signaling downstream of IKK activation. Due to the reduced activity of IKK, pretreating cells with 40 μ M PS1145 significantly reduced NF- κ B translocation by LPS stimulation (Figures S6C and S6D). To test the impact of IKK inhibition for attenuation of subsequent signaling events, we washed cells to remove the drug after LPS stimulation and restimulated with 3 ng/mL (high dose) IL-1 β . Cells treated with PS1145 showed significantly stronger NF- κ B responses to subsequent IL-1 β stimulus compared with untreated cells (Figure 5A). Thus, aspects of NF- κ B signaling downstream of IKK activation, e.g., NF- κ B nuclear translocation and NF- κ B-mediated gene expression, play a major role in LPS-dependent attenuation of subsequent signaling. Through these inhibition studies, we show that asymmetric attenuation of MyD88-dependent signaling depends on IKK activation and subsequent NF- κ B nuclear translocation, suggesting that this asymmetry depends on NF- κ B-mediated gene expression.

Mathematical modeling with two negative feedback motifs reproduces ligand and dose-specific attenuation

Our data give rise to a model where, at high dose, IRAK1 auto-inhibition results in symmetric attenuation of MyD88-dependent signaling, while at moderate and low doses differential transcription of downstream negative regulators produces asymmetric attenuation. To study whether a network topology with these two motifs is sufficient to reproduce our observed prior history effects, we incorporated these two feedbacks into the NF- κ B network model supplemental information (STAR methods) and studied the change in network dynamics when stimulated with different ligand sequences.

To focus on the role of these two negative feedbacks, we minimized the network topology by converging all kinases not

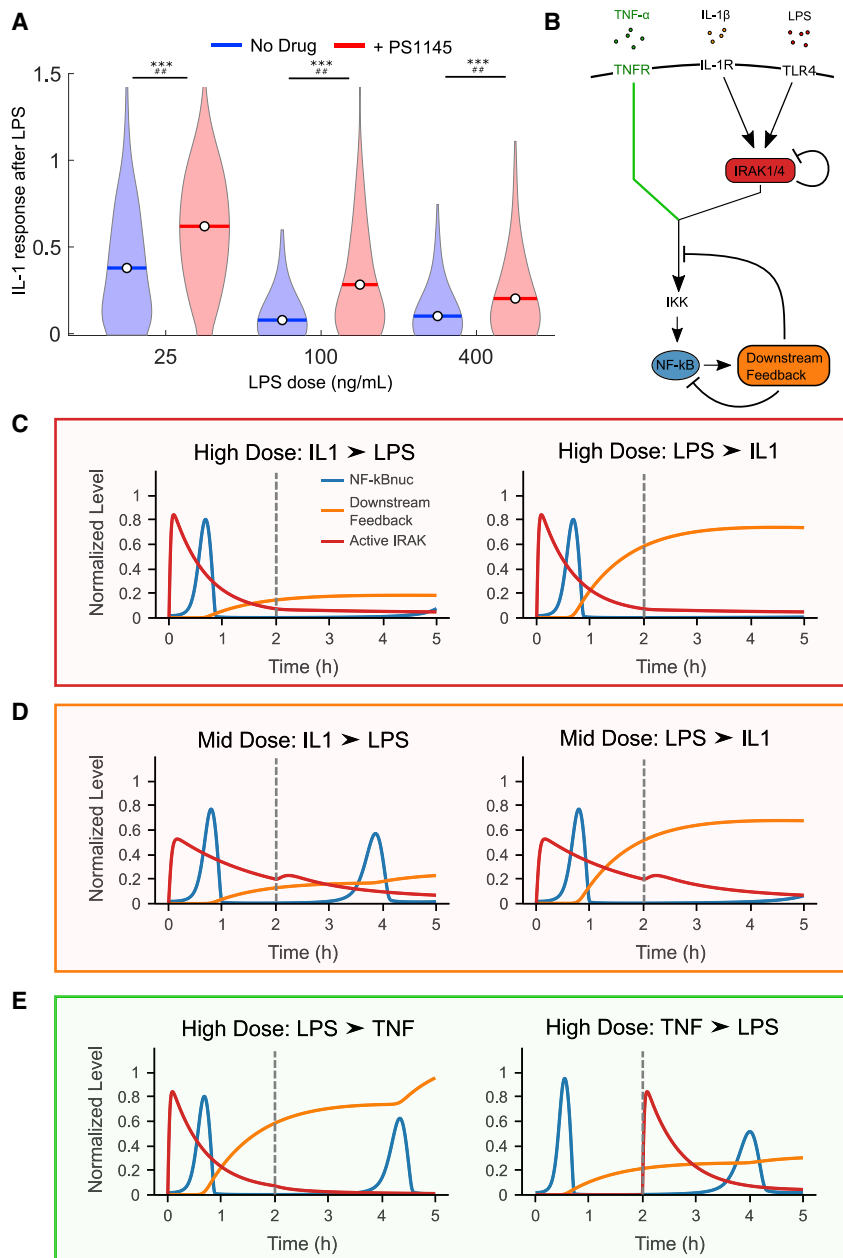


Figure 5. Differential regulation of downstream feedback controls ligand specificity of tolerance

(A) Violin plot comparing IL-1β maximum response following LPS treatment normalized to naive for untreated (blue) and PS1145 pre-treated (red) cells. Pre-treated cells were exposed to 40 μM PS1145 stimulated with LPS at the indicated concentration, washed, and stimulated with 3 ng/mL IL-1β. Each condition shown from >120 single cells over 2 biological replicates. Bonferroni corrected Wilcoxon rank-sum test; ***p < 1 × 10⁻⁴. Fold change difference between sample means >1.25 (##).

(B) Diagram illustrating the NF-κB network model used for the simulation. Two negative components, IRAK1 auto-inhibition and nuclear NF-κB-dependent attenuation, are highlighted in red and orange. The TNF-α signaling pathway (green) utilizes different kinases to activate IKK than the MyD88-dependent ligands.

(C–E) Simulated network responses to different sequences of stimuli. The blue lines show the dynamics of nuclear NF-κB, the red lines for active IRAK1, and the orange lines for the downstream feedback component. Gray dashed vertical line indicates time of simulated replacement of ligands. See also Figures S6C and S6D.

IL-1β or LPS, strong activation of IRAK1 resulted in rapid inactivation, which prevented NF-κB activation by subsequent MyD88 ligands (Figure 5C). However, TNF-α does not affect IRAK1 and only weakly attenuates subsequent signaling due to induction of downstream feedback (Figure 5E).

In contrast, at mid dose, IL-1β induced weaker activation of IRAK1 and resulted in modest inactivation of itself, allowing activation of IRAK1 by subsequent LPS stimulus (Figure 5D). Partial inactivation of IRAK1 by LPS stimulus combined with induction of transcriptional feedback prevented subsequent MyD88-dependent signaling (Figure 5D). Thus, in this dose range, differential engagement of downstream feedback plays a critical role in differentiating LPS and IL-1β signaling and promoting asymmetric response. In

addition, we simulated other six combinations of sequential stimuli (Figure S7A), which reproduced the remaining experimental results.

involved in negative feedback or the translocation of NF-κB (Krishna et al., 2006). Then, we expanded this minimal NF-κB model by adding network components connecting three receptors (TNFR, IL-1R, and TLR4) and incorporating auto-inhibition of IRAK1 and ligand-dependent inhibition downstream of NF-κB (Figure 5B). To model the greater transcription of negative regulators following LPS stimulation compared with IL-1β and TNF-α (Figures 5A and 6C) (Sen et al., 2020), we set the LPS-dependent inhibition arising from NF-κB-dependent transcription to be 4-fold that of IL-1β or TNF-α. Even with these expansions, our model uses only 20 parameters and successfully reproduced our experimental observations (Figures 5C–5E). At high dose of

An alternative mechanism for attenuation is the saturation of signaling molecules shared with the prior stimulus. This possibility is unlikely in our mid- and low-dose situations, as NF-κB signaling was not saturated and clear asymmetry between ligands with comparable NF-κB responses existed. However, at high dose, saturation of NF-κB signaling suggested that reservoirs of intermediaries may be depleted. While this is difficult to test experimentally, our simulation suggests that this mechanism may be possible. Negative feedback on IRAK1 occurs in

the form of auto-inactivation. As a result, high-dose stimulus triggers rapid inactivation of the IRAK1 population, leading to depletion of available IRAK1 (Figure S7B). Although reservoirs of downstream modules, such as IKK, are still available, depletion of IRAK1 prevents further activation through the MyD88-dependent pathway (Figure S7B). Thus, saturation and depletion of shared upstream intermediaries, such as IRAK1, may play a role in attenuation under saturating signaling conditions. At mid dose, however, both IRAK1 and IKK are available following both IL-1 β and LPS stimulus (Figures S7C and S7D). Our simulation demonstrates how a simple network motif with a few negative feedbacks acting on different nodes can retain information about stimulus history and coordinate subsequent inflammatory signaling.

MyD88-dependent ligands differentially regulate NF- κ B response genes associated with negative feedback

Our computational and experimental results suggest that NF- κ B-induced negative feedbacks are differentially regulated by MyD88-dependent ligands. To confirm this model, we profiled gene expression through RNA sequencing following 2 h of stimulation with mid-dose LPS, PAM, or IL-1 β . Compared with unstimulated cells, we found a total of 609 differentially expressed genes (DEGs) following LPS stimulus, 166 following PAM stimulus, and 108 following IL-1 β stimulus (Table S1). Almost all DEGs induced by IL-1 β and PAM were also induced by LPS, while DEGs by IL-1 β and PAM showed little overlap (Figure 6A). Differences in gene expression between these three ligands were primarily driven by magnitude of up- or downregulation, rather than regulation of different genes (Figure 6B). In general, upregulation of gene expression by LPS was stronger than upregulation by PAM, which was itself stronger than by IL-1 β . These differences in the magnitude of gene expression suggest that MyD88-dependent ligands indeed differentially regulate expression of NF- κ B response genes despite highly shared pathways.

We then focused on which genes were most differentially regulated by MyD88 ligands. We found that many known negative regulators of NF- κ B signaling were upregulated 2- to 4-fold in response to LPS stimulus compared with IL-1 β stimulus (Figure 6C). Many of these regulatory genes act to directly sequester NF- κ B or inhibit the activities of shared upstream signaling components (Renner and Schmitz, 2009). Thus, these negative regulators likely affect subsequent signaling by other MyD88 ligands. We also found that the most differentially expressed genes between LPS and IL-1 β are signaling proteins, indicating that these transcriptional differences give rise to different functional outcomes between LPS and IL-1 β signaling (Figure 6D). For example, some of the most differentially regulated genes were well-known proteins secreted by activated fibroblasts, including the growth factors *Csf2* and *Csf3* and the cytokines *Cxcl2* and *Cxcl3* (Bunting et al., 2007; Nishizawa and Nagata, 1990; Widmer et al., 1993).

It is surprising that LPS and IL-1 β induce different gene expression patterns despite similar intracellular pathways. Ligand-specific NF- κ B activation dynamics may be involved in differentiating these expression patterns. LPS consistently produced a longer NF- κ B activation duration than a comparable dose of IL-1 β (Figure S7F). The duration of NF- κ B activation

has been shown to differentially regulate transcription of NF- κ B response genes (Cheng et al., 2021; Sen et al., 2020), possibly explaining differences between IL-1 β - and LPS-induced gene expression. However, longer activation duration also increases the total nuclear NF- κ B over time.

To examine if total nuclear NF- κ B, as measured by the AUC of the NF- κ B response, can explain the differential gene expression by different ligands, we quantified gene expression in cells stimulated with mid-dose IL-1 β and LPS (0.2 and 100 ng/mL, respectively) and a higher dose of IL-1 β (1 ng/mL). Mid-dose IL-1 β produced lower AUC than mid-dose LPS did, while 1 ng/mL IL-1 β produced a similar AUC to mid-dose LPS (Figure 7G). If higher total nuclear NF- κ B explains stronger gene expression by mid-dose LPS than by mid-dose IL-1 β , 1 ng/mL IL-1 β should induce comparable downstream gene expression. Through qRT-PCR, we profiled the transcription of three differentially expressed negative feedback regulators, *Nfkbia*, *Nfkbie*, and *Tnfaip3*. We found that, for *Nfkbia* and *Tnfaip3*, expression was significantly increased in the 100 ng/mL LPS sample compared with both 0.2 and 1 ng/mL IL-1 β samples (Figure 6E). A 0.2 ng/mL IL-1 β stimulus produced weaker expression of *Nfkbia* and *Tnfaip3* compared with untreated cells after 2 h of stimulus. Because these are early NF- κ B target genes which are rapidly transcribed and degraded following activation of NF- κ B, this result is likely due to targeted degradation after an initial burst of transcription (Tay et al., 2010). Importantly, even 1 ng/mL IL-1 β stimulus, which induced comparable NF- κ B response AUC to mid-dose LPS, did not increase transcription of negative regulators of NF- κ B to the level of LPS stimulation.

Similarly, we profiled five secreted proteins that were also highly differentially expressed between LPS and IL-1 β stimulus, *Csf2*, *Csf3*, *Cxcl2*, *Cxcl3*, and *Il23a*. Each of these genes except *Csf3* was significantly upregulated following LPS stimulation compared with both IL-1 β doses. These results suggest that AUC cannot explain the differential downstream expression we observed, but that NF- κ B dynamic features, likely including activation duration, drive the differential downstream expression between LPS and IL-1 β . Similar to what we observed using qPCR, the greater number of DEGs following LPS stimulus may be explained by the difference in activation duration between the LPS and IL-1 β response. Overall, our downstream analyses demonstrate that each MyD88-dependent ligand differentially regulates downstream gene expression, and that differences in negative feedback expression can store prior ligand information to control subsequent NF- κ B signaling.

DISCUSSION

Cells involved in innate immunity must interpret a complex and evolving milieu of extracellular cytokines and pathogenic signals. Despite the temporal features of these challenges, how prior history of inflammatory stimulus reshapes cellular responses to subsequent stimuli remains unclear. Here, we combined microfluidics and live-cell tracking of canonical NF- κ B signaling to track the effects of complex stimulus patterns on inflammatory signaling over the course of hours.

Our results showed that different levels of overlap between ligand pathways and negative feedback modules encode

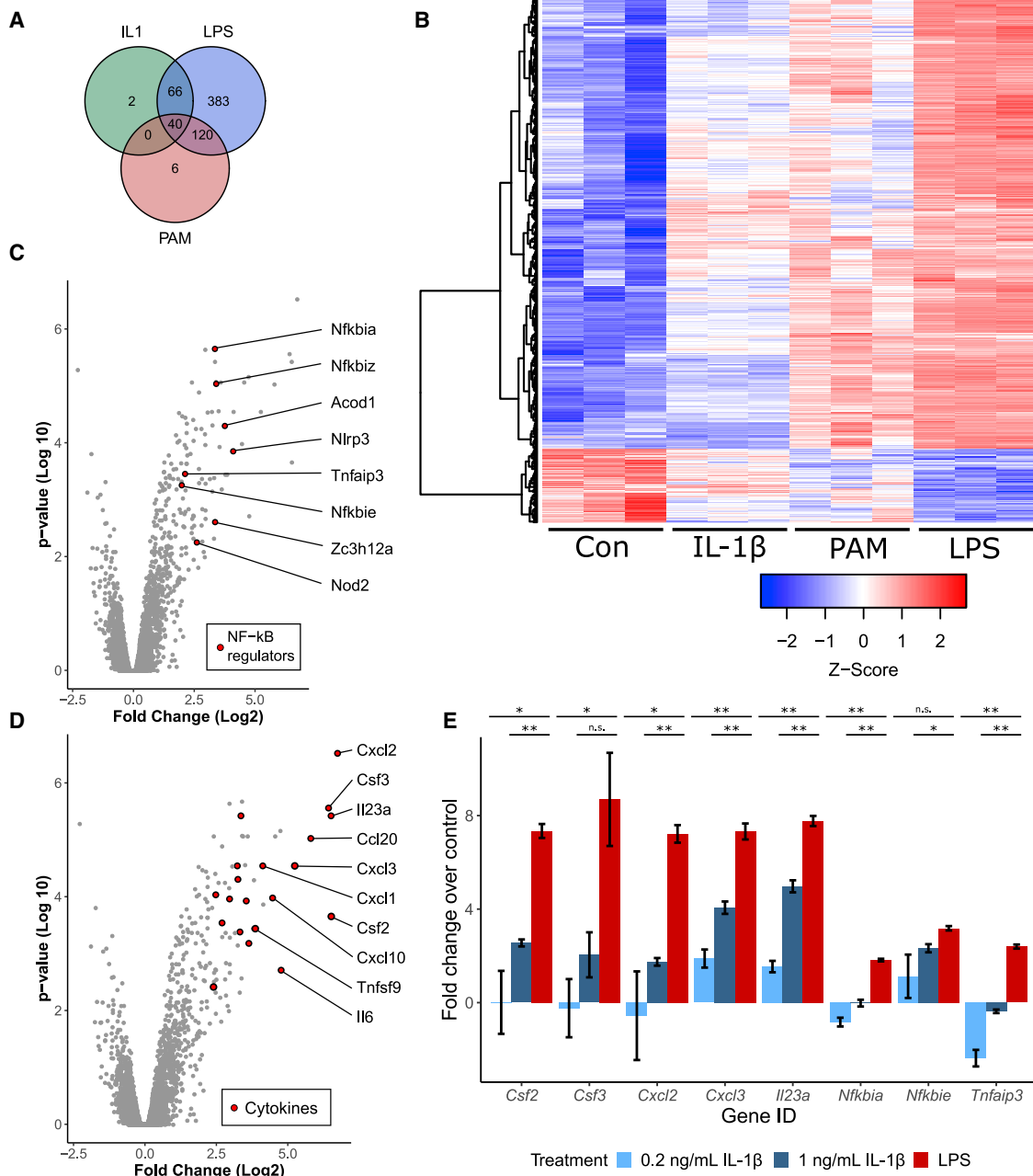


Figure 6. Myd88-dependent genes differentially regulate downstream cytokines and negative feedback regulators

(A) Venn diagram showing overlap of differentially expressed genes (DEGs) between IL-1 β , LPS, and PAM after 2 h of stimulus.

(B) Heatmap of DEGs for MyD88-dependent ligand-treated cells. RNA sequencing was performed in triplicate. Each row shows the normalized expression (Z score) of a single gene. Dendrogram shows linkage based on Ward's method.

(C and D) Volcano plot showing log₂(fold change) and -log₁₀(p value) for DEGs between LPS and IL-1 β stimulus. Among the DEGs with adjusted p < 0.01 and fold change > 4, genes annotated as NF- κ B negative regulators (GO:0032088) (C) or cytokines (GO:0005125) (D) are colored in red. All differentially expressed regulators and top 10 differentially expressed cytokines are labeled.

(E) qRT-PCR data following for a subset of highly differentially expressed cytokines and NF- κ B negative regulators stimulation with 0.2 ng/mL (light blue), 1 ng/mL (dark blue) IL-1 β , or 100 ng/mL LPS (red). Gene expression is normalized to basal gene expression for unstimulated cells. Data shown as mean fold change over unstimulated cells \pm SEM from three replicates. Benjamini-Hochberg adjusted *p < 0.05 or **p < 0.01. See also Figure S7 and Table S1.

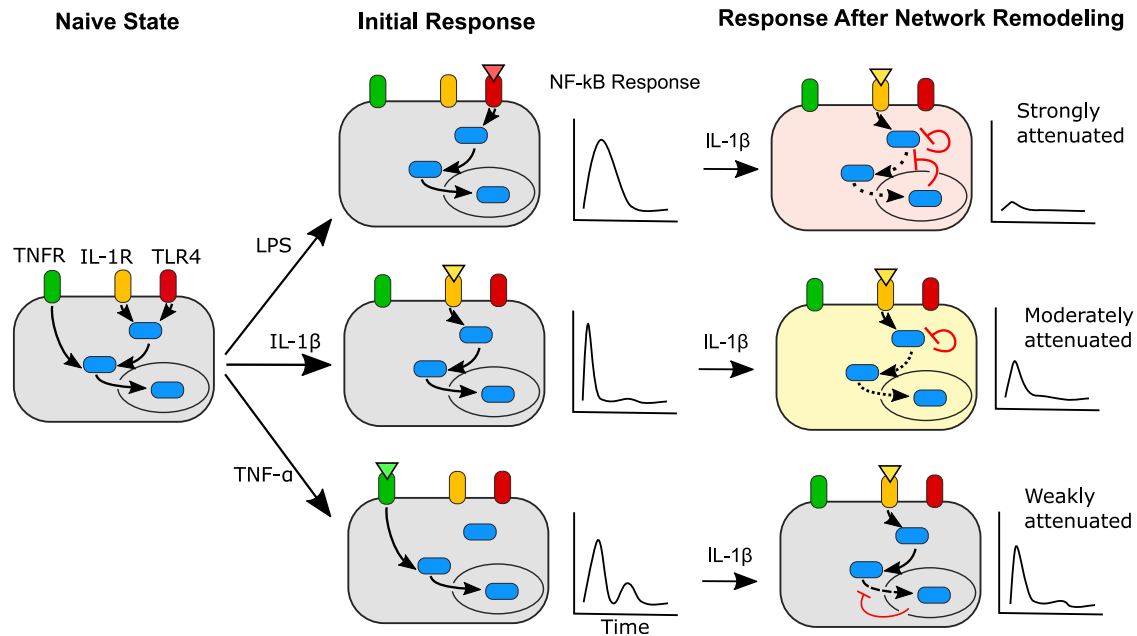


Figure 7. Exposure to inflammatory ligands triggers shared feedbacks to alter subsequent ligand responses

Naive cell (gray) activates in response to different inflammatory ligands, which each induce characteristic feedback responses. LPS (red cell) induces upstream and downstream negative feedback, IL-1 β (yellow cell) primarily induces upstream negative feedback, and TNF- α induces negative feedback, which primarily acts orthogonally to the other ligands. As a result, response to a subsequent IL-1 β stimulus becomes attenuated in a ligand-specific manner and produces memory-informed NF- κ B responses.

information about prior history and shape response to subsequent ligands. TNF- α permits signaling from subsequent ligands and is least affected by prior stimulus history. In contrast, prior history between MyD88-dependent ligands is differentiated by dose-dependent engagement of shared IRAK1 auto-inhibition and ligand-dependent production of downstream negative feedbacks. The combination of these three network features differentiates response dynamics to subsequent ligands based on prior history, even between highly shared pathways, such as IL-1 β and LPS.

Thus, we propose a model of acute memory of prior history in the NF- κ B network where ligand-specific engagement of negative feedbacks acts on nodes of the NF- κ B network shared with subsequent ligands (Figure 7). Memory reshapes the response to the subsequent stimulus, resulting in significantly different NF- κ B activation dynamics. While these dynamics have been extensively shown to control transcriptional outcomes and cell fate (Cheng et al., 2021; Purvis et al., 2012; Sen et al., 2020), we show that they can reflect state changes due to prior stimuli. In future study of innate immune memory, feedback and dynamics in signaling networks should therefore be considered as potential regulatory mechanisms for biological function.

It is notable that we primarily observe tolerance in the time-scales studied, especially as priming has been described using the same ligands (Deng et al., 2013; Fu et al., 2012). These studies, however, describe priming at long time intervals (>24 h) in macrophages. Although the circuit topologies we study give rise to short-term tolerance due to the negative feedback, it may be possible that pathway crosstalk and chromatin/DNA

modifications give rise to long-term priming. Furthermore, proposed circuit motifs for priming involve crosstalk between the NF- κ B pathway and orthogonal pathways not present in fibroblasts (Fu et al., 2012). In myeloid cells, the regulation of innate immune memory by feedback-dependent alteration of NF- κ B dynamics may be further enhanced by cell-type-specific sources of negative and positive feedback (Deng et al., 2013; Janssens et al., 2003). Nonetheless, we show that regulation of the magnitude of tolerance is sufficient to encoding memory of prior stimuli.

Thus, our finding that acute prior history effects are encoded in the dynamic NF- κ B response also presents a form of innate immune memory that acts directly on signal transduction pathways. In addition to epigenetic effects acting on the accessible chromatin landscape of the cell, which occur over days, innate immune memory can also be encoded by NF- κ B dynamics regulated through rapid feedback responses in the upstream signaling network.

Limitations of the study

In this work, we focus on the effect of prior ligands on subsequent ligands of the same approximate dose. It may be possible that additional memory effects may be observed if ligands and doses are mixed in a systematic manner, as the NF- κ B network has been shown to exhibit ligand-specific dose-sensing mechanisms (Son et al., 2021). Furthermore, specialized sentinel cells, such as macrophages and dendritic cells express a far more complete set of receptors and network components that encode responses to inflammatory stimuli (Janssens et al., 2003; Kobayashi et al., 2002). Future study of feedback dynamics will

need to consider the ways in which these specialized cell types may differentially encode memory of prior stimuli. Future experiments using primary tissue from transgenic mice expressing endogenously tagged signaling reporters will be vital to this work (Adelaja et al., 2021; Pokrass et al., 2020). Ultimately, relevance of memory encoding in NF- κ B dynamics will require demonstration that these types of memory encoding occur in physiologically relevant contexts. These studies will likely require *in vivo* physiological models of disease and intravital imaging of NF- κ B dynamics.

STAR★METHODS

Detailed methods are provided in the online version of this paper and include the following:

- **KEY RESOURCES TABLE**
- **RESOURCE AVAILABILITY**
 - Lead contact
 - Materials availability
 - Data and code availability
- **EXPERIMENTAL MODEL AND SUBJECT DETAILS**
 - Cells
- **METHOD DETAILS**
 - Microfluidic device design and fabrication
 - Microfluidic experiment setup
 - Stimulus conditions
 - Image acquisition and analysis
 - CRISPR-Cas9 knockout of MyD88
 - Cell retrieval from microfluidic device for downstream gene measurements
 - Library preparation and RNA-sequencing
 - cDNA synthesis and qPCR
 - NF- κ B network simulation
 - Information theory analysis
- **QUANTIFICATION AND STATISTICAL ANALYSIS**

SUPPLEMENTAL INFORMATION

Supplemental information can be found online at <https://doi.org/10.1016/j.celrep.2022.111159>.

ACKNOWLEDGMENTS

We thank laboratory members for critical reading and discussion of this work. We also thank Markus Covert (Stanford) and Sergi Regot (Johns Hopkins) for providing the cell line used in this study, and Alexander Hoffmann (UCLA) and Roy Wollman (UCLA) for providing the information theory code that our analyses were based on. A.G.W. is supported by the NIH MSTP training grant T32GM07281. This work is supported by NIH grants R01GM128042 and 75N93019C00041, and Army Research Office grant 73231-EL (to S.T.). We thank the University of Chicago Genomics Facility (RRID: SCR_019196) for their assistance with library prep and sequencing. qPCR was performed at the Single Cell Immunophenotyping Core of the University of Chicago.

AUTHOR CONTRIBUTIONS

A.G.W. and M.S. designed and performed the microfluidics experiments with assistance from E.K. A.G.W. and M.S. analyzed the microfluidic data with help from N.T. A.G.W. performed the gene expression analyses with help from M.S.

M.S. built the mathematical models and information theory analyses. S.T. supervised the work. All authors contributed to writing of the manuscript.

DECLARATION OF INTERESTS

The authors declare no competing interests.

Received: February 22, 2022

Revised: May 11, 2022

Accepted: July 13, 2022

Published: August 16, 2022

REFERENCES

- Adamson, A., Boddington, C., Downton, P., Rowe, W., Bagnall, J., Lam, C., Maya-Mendoza, A., Schmidt, L., Harper, C.V., Spiller, D.G., et al. (2016). Signal transduction controls heterogeneous NF- κ B dynamics and target gene expression through cytokine-specific refractory states. *Nat. Commun.* 7, 12057. <https://doi.org/10.1038/ncomms12057>.
- Adelaja, A., Taylor, B., Sheu, K.M., Liu, Y., Luecke, S., and Hoffmann, A. (2021). Six distinct NF κ B signaling codons convey discrete information to distinguish stimuli and enable appropriate macrophage responses. *Immunity* 54, 916–930.e7. <https://doi.org/10.1016/j.immuni.2021.04.011>.
- Ashall, L., Horton, C.A., Nelson, D.E., Paszek, P., Harper, C.V., Sillitoe, K., Ryan, S., Spiller, D.G., Unitt, J.F., Broomhead, D.S., et al. (2009). Pulsatile stimulation determines timing and specificity of NF-kappa B-dependent transcription. *Science* 324, 242–246. <https://doi.org/10.1126/science.1164860>.
- Behar, M., and Hoffmann, A. (2013). Tunable signal processing through a kinase control cycle: the IKK signaling node. *Biophys. J.* 105, 231–241. <https://doi.org/10.1016/j.bpj.2013.05.013>.
- Bunting, K., Rao, S., Hardy, K., Woltring, D., Denyer, G.S., Wang, J., Gerondakis, S., and Shannon, M.F. (2007). Genome-wide analysis of gene expression in T cells to identify targets of the NF-kappa B transcription factor c-Rel. *J. Immunol.* 178, 7097–7109. <https://doi.org/10.4049/jimmunol.178.11.7097>.
- Butcher, S.K., O'Carroll, C.E., Wells, C.A., and Carmody, R.J. (2018). Toll-like receptors drive specific patterns of tolerance and training on restimulation of macrophages. *Front. Immunol.* 9. <https://doi.org/10.3389/fimmu.2018.00933>.
- Cheng, Q.-J., Ohta, S., Sheu, K.M., Spreafico, R., Adelaja, A., Taylor, B., and Hoffmann, A. (2021). NF- κ B dynamics determine the stimulus specificity of epigenomic reprogramming in macrophages. *Science* 372, 1349–1353. <https://doi.org/10.1126/science.abc0269>.
- Cheong, R., Rhee, A., Wang, C.J., Nemenman, I., and Levchenko, A. (2011). Information transduction capacity of noisy biochemical signaling networks. *Science* 334, 354–358. <https://doi.org/10.1126/science.1204553>.
- Cohen, P. (2014). The TLR and IL-1 signalling network at a glance. *J. Cell Sci.* 127, 2383–2390. <https://doi.org/10.1242/jcs.149831>.
- DeFelice, M.M., Clark, H.R., Hughey, J.J., Maayan, I., Kudo, T., Gutschow, M.V., Covert, M.W., and Regot, S. (2019). NF- κ B signaling dynamics is controlled by a dose-sensing autoregulatory loop. *Sci. Signal.* 12, eaau3568. <https://doi.org/10.1126/scisignal.aau3568>.
- Delhase, M., Hayakawa, M., Chen, Y., and Karin, M. (1999). Positive and negative regulation of I κ B kinase activity through IKKbeta subunit phosphorylation. *Science* 284, 309–313. <https://doi.org/10.1126/science.284.5412.309>.
- Deng, H., Maitra, U., Morris, M., and Li, L. (2013). Molecular mechanism responsible for the priming of macrophage activation. *J. Biol. Chem.* 288, 3897–3906. <https://doi.org/10.1074/jbc.M112.424390>.
- Divangahi, M., Aaby, P., Khader, S.A., Barreiro, L.B., Bekkering, S., Chavakis, T., van Crevel, R., Curtis, N., DiNardo, A.R., Dominguez-Andres, J., et al. (2021). Trained immunity, tolerance, priming and differentiation: distinct immunological processes. *Nat. Immunol.* 22, 2–6. <https://doi.org/10.1038/s41590-020-00845-6>.
- Elowitz, M.B., Levine, A.J., Siggia, E.D., and Swain, P.S. (2002). Stochastic gene expression in a single cell. *Science* 297, 1183–1186. <https://doi.org/10.1126/science.1070919>.

- Fitzgerald, K.A., Rowe, D.C., Barnes, B.J., Caffrey, D.R., Visintin, A., Latz, E., Monks, B., Pitha, P.M., and Golenbock, D.T. (2003). LPS-TLR4 signaling to IRF-3/7 and NF- κ B involves the toll Adapters TRAM and TRIF. *J. Exp. Med.* **198**, 1043–1055. <https://doi.org/10.1084/jem.20031023>.
- Foster, S.L., Hargreaves, D.C., and Medzhitov, R. (2007). Gene-specific control of inflammation by TLR-induced chromatin modifications. *Nature* **447**, 972–978. <https://doi.org/10.1038/nature05836>.
- Fu, Y., Glaros, T., Zhu, M., Wang, P., Wu, Z., Tyson, J.J., Li, L., and Xing, J. (2012). Network topologies and dynamics leading to endotoxin tolerance and priming in innate immune cells. *PLoS Comput. Biol.* **8**, e1002526. <https://doi.org/10.1371/journal.pcbi.1002526>.
- Gómez-Sjöberg, R., Leyrat, A.A., Pirone, D.M., Chen, C.S., and Quake, S.R. (2007). Versatile, fully automated, microfluidic cell culture system. *Anal. Chem.* **79**, 8557–8563. <https://doi.org/10.1021/ac071311w>.
- Hackett, T.-L., Holloway, R., Holgate, S.T., and Warner, J.A. (2008). Dynamics of pro-inflammatory and anti-inflammatory cytokine release during acute inflammation in chronic obstructive pulmonary disease: an ex vivo study. *Respir. Res.* **9**, 47. <https://doi.org/10.1186/1465-9921-9-47>.
- Hayden, M.S., and Ghosh, S. (2012). NF- κ B, the first quarter-century: remarkable progress and outstanding questions. *Genes Dev.* **26**, 203–234. <https://doi.org/10.1101/gad.183434.111>.
- Heremans, H., Van Damme, J., Dillen, C., Dijkmans, R., and Billiau, A. (1990). Interferon gamma, a mediator of lethal lipopolysaccharide-induced Shwartzman-like shock reactions in mice. *J. Exp. Med.* **171**, 1853–1869. <https://doi.org/10.1084/jem.171.6.1853>.
- Hoffmann, A., Levchenko, A., Scott, M.L., and Baltimore, D. (2002). The I κ B-NF- κ B signaling module: temporal control and selective gene activation. *Science* **298**, 1241–1245. <https://doi.org/10.1126/science.1071914>.
- Ifrim, D.C., Quintin, J., Joosten, L.A.B., Jacobs, C., Jansen, T., Jacobs, L., Gow, N.A.R., Williams, D.L., Meer, J.W.M. van der, and Netea, M.G. (2014). Trained immunity or tolerance: opposing functional programs induced in human monocytes after engagement of various pattern recognition receptors. *Clin. Vaccine Immunol.* **21**, 534–545. <https://doi.org/10.1128/CVI.00688-13>.
- Janssens, S., Burns, K., Vercammen, E., Tschopp, J., and Beyaert, R. (2003). MyD88S, a splice variant of MyD88, differentially modulates NF- κ B- and AP-1-dependent gene expression. *FEBS (Fed. Eur. Biochem. Soc.) Lett.* **548**, 103–107. [https://doi.org/10.1016/S0014-5793\(03\)00747-6](https://doi.org/10.1016/S0014-5793(03)00747-6).
- Kawasaki, T., and Kawai, T. (2014). Toll-like receptor signaling pathways. *Front. Immunol.* **0**. <https://doi.org/10.3389/fimmu.2014.00461>.
- Kearns, J.D., Basak, S., Werner, S.L., Huang, C.S., and Hoffmann, A. (2006). I κ B β provides negative feedback to control NF- κ B oscillations, signaling dynamics, and inflammatory gene expression. *J. Cell Biol.* **173**, 659–664. <https://doi.org/10.1083/jcb.200510155>.
- Kellogg, R.A., and Tay, S. (2015). Noise facilitates transcriptional control under dynamic inputs. *Cell* **160**, 381–392. <https://doi.org/10.1016/j.cell.2015.01.013>.
- Kellogg, R.A., Gómez-Sjöberg, R., Leyrat, A.A., and Tay, S. (2014). High-throughput microfluidic single-cell analysis pipeline for studies of signaling dynamics. *Nat. Protoc.* **9**, 1713–1726. <https://doi.org/10.1038/nprot.2014.120>.
- Kellogg, R.A., Tian, C., Eitzrodt, M., and Tay, S. (2017). Cellular decision making by non-integrative processing of TLR inputs. *Cell Rep.* **19**, 125–135. <https://doi.org/10.1016/j.celrep.2017.03.027>.
- Kiers, D., Koch, R.M., Hamers, L., Gerretsen, J., Thijs, E.J.M., van Ede, L., Riksen, N.P., Kox, M., and Pickkers, P. (2017). Characterization of a model of systemic inflammation in humans in vivo elicited by continuous infusion of endotoxin. *Sci. Rep.* **7**, 40149. <https://doi.org/10.1038/srep40149>.
- Kobayashi, K., Hernandez, L.D., Galán, J.E., Janeway, C.A., Medzhitov, R., and Flavell, R.A. (2002). IRAK-M is a negative regulator of toll-like receptor signaling. *Cell* **110**, 191–202. [https://doi.org/10.1016/S0092-8674\(02\)00827-9](https://doi.org/10.1016/S0092-8674(02)00827-9).
- Krishna, S., Jensen, M.H., and Sneppen, K. (2006). Minimal model of spiky oscillations in NF- κ B signaling. *Proc. Natl. Acad. Sci. USA* **103**, 10840–10845. <https://doi.org/10.1073/pnas.0604085103>.
- Kudo, T., Jeknić, S., Macklin, D.N., Akhter, S., Hughey, J.J., Regot, S., and Covert, M.W. (2018). Live-cell measurements of kinase activity in single cells using translocation reporters. *Nat. Protoc.* **13**, 155–169. <https://doi.org/10.1038/nprot.2017.128>.
- Lawrence, T. (2009). The nuclear factor NF- κ B pathway in inflammation. *Cold Spring Harb Perspect Biol.* **1**, a001651. <https://doi.org/10.1101/cshperspect.a001651>.
- Lérias, J.R., de Sousa, E., Paraschoudi, G., Martins, J., Condeço, C., Figueiredo, N., Carvalho, C., Doodoo, E., Maia, A., Castillo-Martin, M., et al. (2020). Trained immunity for personalized cancer immunotherapy: current knowledge and future opportunities. *Front. Microbiol.* **0**. <https://doi.org/10.3389/fmicb.2019.02924>.
- Luan, H.H., Wang, A., Hilliard, B.K., Carvalho, F., Rosen, C.E., Ahasic, A.M., Herzog, E.L., Kang, I., Pisani, M.A., Yu, S., et al. (2019). GDF15 is an inflammation-induced central mediator of tissue tolerance. *Cell* **178**, 1231–1244.e11. <https://doi.org/10.1016/j.cell.2019.07.033>.
- Newman, J.R.S., Ghaemmaghami, S., Ihmels, J., Breslow, D.K., Noble, M., DeRisi, J.L., and Weissman, J.S. (2006). Single-cell proteomic analysis of *S. cerevisiae* reveals the architecture of biological noise. *Nature* **441**, 840–846. <https://doi.org/10.1038/nature04785>.
- Nishizawa, M., and Nagata, S. (1990). Regulatory elements responsible for inducible expression of the granulocyte colony-stimulating factor gene in macrophages. *Mol. Cell Biol.* **10**, 2002–2011. <https://doi.org/10.1128/mcb.10.5.2002-2011.1990>.
- Novakovic, B., Habibi, E., Wang, S.-Y., Arts, R.J.W., Davar, R., Megchelenbrink, W., Kim, B., Kuznetsova, T., Kox, M., Zwaag, J., et al. (2016). β -Glucan reverses the epigenetic state of LPS-induced immunological tolerance. *Cell* **167**, 1354–1368, e14. <https://doi.org/10.1016/j.cell.2016.09.034>.
- Phelps, C.B., Sengchanthalangsy, L.L., Malek, S., and Ghosh, G. (2000). Mechanism of κ B DNA binding by Rel/NF- κ B dimers. *J. Biol. Chem.* **275**, 24392–24399. <https://doi.org/10.1074/jbc.M003784200>.
- Pokrass, M.J., Ryan, K.A., Xin, T., Pielstick, B., Timp, W., Greco, V., and Regot, S. (2020). Cell-cycle-dependent ERK signaling dynamics direct fate specification in the mammalian preimplantation embryo. *Dev. Cell* **55**, 328–340.e5. <https://doi.org/10.1016/j.devcel.2020.09.013>.
- Pulendran, B., Arunachalam, P.S., and O’Hagan, D.T. (2021). Emerging concepts in the science of vaccine adjuvants. *Nat. Rev. Drug Discov.* **20**, 454–475. <https://doi.org/10.1038/s41573-021-00163-y>.
- Purvis, J.E., Karhohs, K.W., Mock, C., Batchelor, E., Loewer, A., and Lahav, G. (2012). p53 dynamics control cell fate. *Science* **336**, 1440–1444. <https://doi.org/10.1126/science.1218351>.
- Rao, P., Hayden, M.S., Long, M., Scott, M.L., West, A.P., Zhang, D., Oeckinghaus, A., Lynch, C., Hoffmann, A., Baltimore, D., et al. (2010). I κ B β acts to inhibit and activate gene expression during the inflammatory response. *Nature* **466**, 1115–1119. <https://doi.org/10.1038/nature09283>.
- Regot, S., Hughey, J.J., Bajar, B.T., Carrasco, S., and Covert, M.W. (2014). High-Sensitivity measurements of multiple kinase activities in live single cells. *Cell* **157**, 1724–1734. <https://doi.org/10.1016/j.cell.2014.04.039>.
- Renner, F., and Schmitz, M.L. (2009). Autoregulatory feedback loops terminating the NF- κ B response. *Trends Biochem. Sci.* **34**, 128–135. <https://doi.org/10.1016/j.tibs.2008.12.003>.
- Selimkhanov, J., Taylor, B., Yao, J., Pilko, A., Albeck, J., Hoffmann, A., Tsimring, L., and Wollman, R. (2014). Accurate information transmission through dynamic biochemical signaling networks. *Science* **346**, 1370–1373. <https://doi.org/10.1126/science.1254933>.
- Sen, S., Cheng, Z., Sheu, K.M., Chen, Y.H., and Hoffmann, A. (2020). Gene regulatory strategies that decode the duration of NF κ B dynamics contribute to LPS- versus TNF-specific gene expression. *Cell Systems* **10**, 169–182.e5. <https://doi.org/10.1016/j.cels.2019.12.004>.
- Shannon, C.E. (1948). A mathematical theory of communication. *Bell System Technical Journal* **27**, 379–423. <https://doi.org/10.1002/j.1538-7305.1948.tb01338.x>.
- Shembade, N., Ma, A., and Harhaj, E.W. (2010). Inhibition of NF- κ B signaling by A20 through disruption of ubiquitin enzyme complexes. *Science* **327**, 1135–1139. <https://doi.org/10.1126/science.1182364>.

- Simpson, M.L., Cox, C.D., Allen, M.S., McCollum, J.M., Dar, R.D., Karig, D.K., and Cooke, J.F. (2009). Noise in biological circuits. *WIREs Nanomedicine and Nanobiotechnology* 1, 214–225. <https://doi.org/10.1002/wnan.22>.
- Son, M., Wang, A.G., Tu, H.-L., Metzigg, M.O., Patel, P., Husain, K., Lin, J., Murgan, A., Hoffmann, A., and Tay, S. (2021). NF- κ B responds to absolute differences in cytokine concentrations. *Sci. Signal.* 14, eaaz4382. <https://doi.org/10.1126/scisignal.aaz4382>.
- Taniguchi, Y., Choi, P.J., Li, G.-W., Chen, H., Babu, M., Hearn, J., Emili, A., and Xie, X.S. (2010). Quantifying *E. coli* proteome and transcriptome with single-molecule sensitivity in single cells. *Science* 329, 533–538. <https://doi.org/10.1126/science.1188308>.
- Tay, S., Hughey, J.J., Lee, T.K., Lipniacki, T., Quake, S.R., and Covert, M.W. (2010). Single-cell NF- κ B dynamics reveal digital activation and analogue information processing. *Nature* 466, 267–271. <https://doi.org/10.1038/nature09145>.
- Tudelska, K., Markiewicz, J., Kocharczyk, M., Czerkies, M., Prus, W., Korwek, Z., Abdi, A., Błoński, S., Kaźmierczak, B., and Lipniacki, T. (2017). Information processing in the NF- κ B pathway. *Sci. Rep.* 7, 15926. <https://doi.org/10.1038/s41598-017-16166-y>.
- Wajant, H., and Scheurich, P. (2011). TNFR1-induced activation of the classical NF- κ B pathway. *FEBS J.* 278, 862–876. <https://doi.org/10.1111/j.1742-4658.2011.08015.x>.
- Werner, S.L., Barken, D., and Hoffmann, A. (2005). Stimulus specificity of gene expression programs determined by temporal control of IKK activity. *Science* 309, 1857–1861. <https://doi.org/10.1126/science.1113319>.
- Widmer, U., Manogue, K.R., Cerami, A., and Sherry, B. (1993). Genomic cloning and promoter analysis of macrophage inflammatory protein (MIP)-2, MIP-1 alpha, and MIP-1 beta, members of the chemokine superfamily of proinflammatory cytokines. *J. Immunol.* 150, 4996–5012.
- Yamamoto, M., Sato, S., Hemmi, H., Hoshino, K., Kaisho, T., Sanjo, H., Takeuchi, O., Sugiyama, M., Okabe, M., Takeda, K., et al. (2003). Role of adaptor TRIF in the MyD88-independent toll-like receptor signaling pathway. *Science* 301, 640–643. <https://doi.org/10.1126/science.1087262>.
- Yemelyanov, A., Gasparian, A., Lindholm, P., Dang, L., Pierce, J.W., Kisseljev, F., Karseladze, A., and Budunova, I. (2006). Effects of IKK inhibitor PS1145 on NF- κ B function, proliferation, apoptosis and invasion activity in prostate carcinoma cells. *Oncogene* 25, 387–398. <https://doi.org/10.1038/sj.onc.1209066>.

STAR★METHODS

KEY RESOURCES TABLE

REAGENT or RESOURCE	SOURCE	IDENTIFIER
Antibodies		
MyD88 (D80F5) Rabbit mAb	Cell Signaling Technologies	Cat. #4283; RRID: AB_10547882
beta Actin Loading Control Monoclonal Antibody (BA3R), DyLight™ 680	Invitrogen	Catalog # MA5-15739-D680; RRID:AB_2537665
Goat anti-Rabbit IgG (H+L) Cross-Adsorbed Secondary Antibody, DyLight™ 800	Invitrogen	Catalog # SA5-10036; RRID:AB_2556616
Chemicals, peptides, and recombinant proteins		
PS 1145 dihydrochloride	Tocris	4569
Ultrapure LPS, E. coli 0111:B4	Invivogen	tlr1-3pelps
PAM2CSK4: Synthetic diacylated lipopeptide; TLR2/TLR6 agonist	Invivogen	tlr1-pm2s-1
Recombinant Mouse TNF-alpha	R&D Systems	aa 80-235
Recombinant Mouse IL-1 beta/IL-1F2 Protein	R&D Systems	401ML010CF
SuperScript™ II Reverse Transcriptase	Invitrogen	18064014
KAPA HiFi HotStart ReadyMix	Roche	HIFI
Recombinant RNase Inhibitor	Takara	2313A
Polydimethylsiloxane	Momentive	RTV-615
Human Plasma Fibronectin Purified Protein	Millipore Sigma	FC010
FluoroBrite™ DMEM	Invitrogen	A1896701
Critical commercial assays		
SuperScript™ III CellsDirect™ cDNA Synthesis Kit	Invitrogen	18080200
Cell Line Nucleofector™ Kit R	Lonza	Catalog #: VVCA-1001
Csf2 PrimeTime probe assay	IDT	Mm.PT.58.10456839
Csf3 PrimeTime probe assay	IDT	Mm.PT.58.43222334.g
Cxcl2 PrimeTime probe assay	IDT	Mm.PT.58.7603454.g
Cxcl3 PrimeTime probe assay	IDT	Mm.PT.58.45877295.g
Il23a PrimeTime probe assay	IDT	Mm.PT.58.10594618.g
Gapdh PrimeTime probe assay	IDT	Mm.PT.39a.1
Nfkb1a TaqMan probe assay	ThermoFisher Scientific	Mm00477798_m1
Nfkb1e TaqMan probe assay	ThermoFisher Scientific	Mm01269649_m1
Nextera XT DNA Library Preparation Kit	Illumina	FC-131-1024
Deposited data		
RNAseq data reported in this paper	This study	GEO: GSE193053
Trace/microscopy data reported in this paper	This study	Github: https://github.com/tay-lab/Sequential_NF-kB_stim ; Zenodo: https://doi.org/10.5281/zenodo.6626195
Experimental models: Cell lines		
p65 ^{-/-} p65-DsRed JNK-KTR NIH3T3 mouse embryonic fibroblasts	Markus Covert (Stanford)	N/A
Oligonucleotides		
Tnfaip3 qPCR FWD: GCAGCTGGAATCTCT GAAATCT	IDT	N/A
Tnfaip3 qPCR REV: AGTTGTCCCATTCGTC ATTCC	IDT	N/A

(Continued on next page)

Continued

REAGENT or RESOURCE	SOURCE	IDENTIFIER
Tnfaip3 qPCR PRB: FAM/AAACAGGAC/ZEN/TTTGCTACGACACTCGG/3IABkFQ/	IDT	N/A
TSO oligo: AAGCAGTGGTATCAACGCAGA GTGAATrGrGrG	IDT	N/A
ISPCR primer: AAGCAGTGGTATCAACGC AGAGT	IDT	N/A
OligodT ₃₀ VN: AAGCAGTGGTATCAACG CAGAGTACTTTTTTTTTTTTTTTTTTTTTT TTTTTTVN	IDT	N/A
MyD88 gRNA template: TCGCGCTTAAC GTGGGAGTG	IDT	N/A
Recombinant DNA		
pX330-U6-Chimeric_BB-CBh-hSpCas9	Addgene	Plasmid #42230
Software and algorithms		
MATLAB R2021b	Mathworks	https://www.mathworks.com/products/matlab.html
RStudio Build 372	RStudio	https://www.rstudio.com/
R version 4.1.2	R-project	https://www.r-project.org/
Python 3.10	Python	https://www.python.org/

RESOURCE AVAILABILITY

Lead contact

Further information and requests for resources and reagents should be directed to the lead contact, Professor Savaş Tay (tays@uchicago.edu).

Materials availability

This study did not generate new unique reagents.

Data and code availability

- RNA-seq data have been deposited at GEO and are publicly available. Accession number is listed in the [key resources table](#). Original western blot images are included in the Supplemental Figures. Microscopy data reported in this paper will be shared by the [lead contact](#) upon request.
- All original code and analyzed image data necessary to reproduce the figures has been deposited in Github and is publicly available as of the date of publication. The link to the Github repository and the Zenodo DOI are listed in the [key resources table](#).
- Any additional information required to reanalyze the data reported in this paper is available from the [lead contact](#) upon request.

EXPERIMENTAL MODEL AND SUBJECT DETAILS

Cells

RelA^{-/-} NIH3T3 immortalized mouse embryonic fibroblasts (3T3s) stably expressing RelA-DsRed, JNK-kinase translocation reporter-mCerulean3 (JNK-KTR) (Regot et al., 2014), and histone 2B-green fluorescent protein (H2B-GFP) were cultured with Dulbecco's Modified Eagle Medium – High Glucose (DMEM; Gibco) supplemented with 10% fetal bovine serum (Omega Scientific), 1% GlutaMAX (Gibco), and 100 u/mL penicillin-streptomycin (Gibco) in tissue-culture treated flasks. Cells were cultured in a tissue culture incubator maintained at 37°C and 5% CO₂. Cells were passed prior to reaching 100% confluency and maintained for no more than 15 passages.

METHOD DETAILS

Microfluidic device design and fabrication

A previously designed and published cell culture device was utilized for automated cell culture and ligand stimulus (Son et al., 2021). The design contains 14 unique stimulus inputs and 64 independently controlled cell culture chambers measuring 3.5 × 0.8 × 0.035 mm, where each can load more than 500 cells. Master molds for this chip were fabricated by patterning photoresist

deposited on silicon wafers through multilayer soft lithography (Gómez-Sjöberg et al., 2007). Microfluidic devices were fabricated by pouring polydimethylsiloxane (PDMS; Momentive, RTV-615) on the control and flow master molds and bonding these two layers. Control layer wafers were poured with 66 g PDMS (10:1 monomer to catalyst), air bubbles removed under vacuum, and cured at 80°C overnight to make a ~2 cm thick PDM slab with the control pattern grooved on the bottom. Flow layer wafers were poured with 15 g PDMS (10:1 monomer to catalyst) and spun at 2200 rpm to achieve a thickness of ~50 μm and cured at 80°C for at least 1 h. After curing, holes intended for control pins were punched in the control layer, both PDM layers were treated with oxygen plasma (Harrick, PDC-001), aligned using a custom stereomicroscope, and the aligned chip were baked at 80°C overnight. After bonding, holes intended for fluid input and output were punched; then the chip was bonded to a glass slide through plasma treatment and baking. A detailed fabrication protocol can be found in our previous publications (Kellogg et al., 2014; Son et al., 2021).

Microfluidic experiment setup

Device control layer inputs were connected to pneumatic solenoid valves with electronic controller boxes. By actuating different sets of valves, flow pathways in the microfluidic device can be directed from a particular input to a particular chamber using pre-written MATLAB scripts and a custom-developed graphic user interface (GUI). The device was mounted on a microscope (Nikon) and cell chambers were filled with 0.25 mg/mL fibronectin (Millipore) in sterile pH 7.4 phosphate buffered saline (PBS, Gibco), and incubated overnight at room temperature. Subsequently, chambers and channels were flushed with complete medium to replace the fibronectin, then the temperature, humidity, and CO₂ in the live imaging apparatus (Life Imaging Services) were set to 37°C, 100% humidity, and 5% CO₂ to optimize cell culturing in the microfluidic device. Cells were harvested with trypsin, washed with complete medium, and resuspended at ~5*10⁶ cells/mL in FluoroBrite DMEM (Gibco) with the same supplements to reduce background fluorescence. Cells were loaded at approximately 50% confluency to optimize tracking efficiency, and cells were allowed to settle and equilibrate for 5 h prior to start of stimulation and imaging.

Stimulus conditions

Four ligands, mouse tumor necrosis factor alpha (TNF-α; R&D Systems, aa 80-235), mouse interleukin 1 beta (IL-1β; R&D Systems, 401ML010CF), ultrapure lipopolysaccharide (LPS) from *E. coli* (InvivoGen, tlr-3pelps), and PAM2CSK4 (PAM; InvivoGen, tlr-pm2s) were utilized in this study. Based on experimental quantification of NF-κB translocation following titration of each ligand, we selected high, mid, and low doses of each ligand with comparable activation (TNF-α: 90, 30, 3 ng/mL; IL-1β: 3, 0.2, 0.05 ng/mL; LPS: 400, 100, 12.5 ng/mL; PAM: 1, 0.1, 0.01 ng/mL). For each set of high, middle, and low dose ligands, all non-repeating combinations of the four ligands were supplied at 2-h intervals, producing 24 conditions per dose over 8 h. One condition was maintained as a positive control (mid dose TNF-α, IL-1β, LPS, PAM) and one condition maintained as a negative control (4 feedings of complete media). For other experimental conditions, ligands were provided and switched at the indicated dose at the indicated time. Ligand dilutions were made from stock solutions stored at -80°C immediately prior to stimulus, stored on ice during the duration of the experiment, and delivered to the chip through polyetheretherketone tubing (VICI, TPK.505). Input pressure was maintained at 4 psi to prevent shear stress on cells during feeding. For IKK inhibition experiments, PS1145 (Tocris, 4569) was diluted in complete media to 40 μM. Cells were pretreated with PS1145 for 90 min, then exposed to media containing PS1145 and LPS for 4 h, washed for 30 min in complete media, and stimulated with IL-1β (3 ng/mL). Other detailed protocols for the microfluidic experiment can be found in our previous publications (Kellogg et al., 2014).

Image acquisition and analysis

Epifluorescence images were acquired using a Nikon Ti2 microscope enclosed within a temperature-controlled incubator (Life Imaging Services). Images were captured at 20X magnification through a complementary metal-oxide semiconductor camera (Hamamatsu, ORCA-Flash4.0 V2) every 6 min. Each chamber position was imaged for p65-DsRed (555-nm excitation, 0.5-1 s exposure time), H2B-GFP (485-nm, 50-100 ms), and/or KTR-JNK-mCerulean3 (440-nm, 100 ms). No photobleaching or phototoxicity was observed over the course of the imaging process. For the time resolved experiments switching from LPS to IL-1β, imaging was conducted every 3 min instead in order to increase the temporal resolution of the trace.

Prior to image processing, background fluorescence and dark frame images were taken for flat field correction. Nuclear and cytoplasmic DsRed and/or mCerulean3 fluorescence for single cells were evaluated over the course of the experiment by analyzing time course fluorescence images with custom developed software (MATLAB). Briefly, H2B-GFP images were used to segment the nuclear region for each cell, whose positions were tracked over the entire sequence of time course images. Combining these single cell trajectories with the DsRed and mCerulean3 images, we quantified the median nuclear fluorescence in the nucleus, which represented the nuclear NF-κB level, and normalized this fluorescence to the median cytoplasmic fluorescence evaluated from a ring of cytoplasm located around the segmented nuclear image (Kudo et al., 2018). To quantify the background fluorescence, a few small regions without cells were randomly selected, and their mean fluorescence were evaluated and subtracted from the corresponding fluorescence measurement. The resulting traces were processed using another custom-developed analysis software to remove traces displaying cell death, division, or other features which impact data quality. Only traces which were complete over the entire course of each experiment were retained for subsequent analysis.

Key trace features were extracted using custom software (MATLAB). The frame of the maximum RelA or JNK-KTR response in a stimulus interval was identified using a trace smoothed with the lowess method with a span size of 3 to reduce noise from cell

movement, slight changes in imaging focus, or background fluctuations. Frames identified from the smoothed trace were then used to identify the true maximum fluorescence in the un-smoothed trace. To account for the possibility of oscillations in nuclear translocation, multiple local maxima were allowed with a minimum distance between maxima of 5 frames (30 min). To distinguish true maxima from noise due to frame-by-frame fluctuation in nuclear fluorescence, we set the 95th percentile of maxima identified from unstimulated cells as the cutoff and set all stimulus maxima below that cutoff to be zero. Area under the curve (AUC) for each stimulus interval was calculated by taking the trapezoidal approximate of the integral for each trace in the defined time interval.

CRISPR-Cas9 knockout of MyD88

A *Myd88*-targeting guide RNA (5'-TCGCGCTTAACGTGGGAGTG-3') was cloned into the pX330 plasmid backbone (Addgene Plasmid #42230) and transfected using electroporation (Lonza) into 3T3s. 48 h post-transfection, single cells were sorted into a 96-well plate and allowed to grow into clonal populations. Screening by Sanger sequencing identified three clones with frameshift mutations in one or both copies of the gene. Successful knockout was confirmed with western blot probing for MyD88 (1° rabbit anti-MyD88 1:1000, Cell Signaling Technologies. 2° goat anti-rabbit DyLight 800 1:25000), following which the blot was stripped and reprobed for β -actin as a loading control (mouse anti- β -Actin DyLight 680, 1:1000). Blots were imaged on a LICOR scanner on the 700 and 800 nm channels.

Cell retrieval from microfluidic device for downstream gene measurements

To facilitate retrieval of cells, the corner of the microfluidic device with the outlet was cut to expose the outlet channel. At the indicated time following stimulation, cells in the target chamber were treated with TrypLE Express (Gibco) for ~1 min to detach them from the treated surface, then sent to the outlet channel by washing with PBS. Detached cells accumulated at the outlet channel, were removed in a ~2 μ L droplet by manual pipetting, and deposited in 10 μ L ice-cold lysis buffer containing 0.1% Triton-X 100 and RNase inhibitor (Takara) and stored at -80°C until further processing. Approximately 1500 cells were retrieved per replicate per condition.

Library preparation and RNA-sequencing

Sample prep for RNA-sequencing followed the SMART-Seq2 pipeline for single cells. Briefly, cell lysate was incubated at 72°C with oligo-dT₃₀VN to anneal, followed by the rest of the SMART-Seq2 reverse transcriptase mix and incubated at 42°C for 90 min followed by 10 cycles between 50°C and 42°C to unfold secondary structure. Template switching using a modified TSO oligo (5'-AA GCAGTGGTATCAACGCAGAGTGAATrGrGrG -3') provided a PCR handle on the 3' end of the newly synthesized cDNA strand. 6 cycles of single primer preamplification with KAPA HiFi (Roche, primer: AAGCAGTGGTATCAACGCAGAGT), and purification with Ampure XP beads (1:1 ratio, Beckman Coulter) produced a purified cDNA library. Library prep was performed by the University of Chicago Genomics Facility using the Nextera XT procedure. Samples were then single end sequenced in the same facility on an Illumina HiSEQ4000 with a read length of 50 bp. Adapter trimming and read mapping to the reference mouse genome (GRCm38) was done using STAR using default parameters. Transcript abundance was quantified using featureCounts. Raw counts were normalized and differential gene expression identified using the R packages edgeR and limma. Differential genes were identified between IL-1 β and untreated, PAM and untreated, LPS and untreated, and IL-1 β and LPS using cutoffs of Benjamini-Hochberg false discovery rate (FDR) < 0.01 and log fold change > 1.

cDNA synthesis and qPCR

Targeted reverse transcription and preamplification were done using a CellDirect One-Step RT-qPCR kit (Thermo Fisher). qPCR was performed with custom primer/probe sets (*Tnfrsf3*, FWD: GCAGCTGGAATCTCTGAAATCT, REV: AGTTGTCCCATTTCG TCATTCC, PRB:/56-FAM/AAACAGGAC/ZEN/TTTGCTACGACACTCGG/3IABKFQ), predesigned IDT PrimeTime probe assays (*Csf2*: Mm.PT.58.10456839, *Csf3*: Mm.PT.58.43222334.g, *Cxcl2*: Mm.PT.58.7603454.g, *Cxcl3*: Mm.PT.58.45877295.g, *Il23a*: Mm.PT.58.10594618.g, *Gapdh*: Mm.PT.39a.1), or predesigned TaqMan probe assays (*Nfkbia*: Mm00477798_m1, *Nfkbie*: Mm01269649_m1). Ct values were calculated using software defaults and normalized to glyceraldehyde-3-phosphate dehydrogenase (GAPDH) expression to produce Δ Ct values. Δ Ct values were subtracted from the Δ Ct values from control samples to calculate the $\Delta\Delta$ Ct as a proxy for fold change expression over control.

NF- κ B network simulation

Building system of equations

To investigate if the two negative feedback model (Figure 4C) is sufficient for the ligand history effect, we built a simplified network simulation. We extended the previous minimal NF- κ B model (Krishna et al., 2006), which comprises three coupled differential equations each describing the dynamics of nuclear NF- κ B (Equation 1), mRNA of I κ B α (Equation 2), and cytoplasmic I κ B α (Equation 3). Previous studies report that nuclear NF- κ B activates the transcription of downstream gene in a sigmoidal fashion with sharp threshold (Kellogg and Tay, 2015; Phelps et al., 2000). Thus, we adapted the Hill function to describe mRNA transcription and applied a Hill coefficient of four to accurately describe the dynamics (Equation 2). Our study involved various ligand stimuli, where each corresponds to different receptor and involves various cytoplasmic kinases for NF- κ B activation. However, all signaling pathways converge on an essential mediator, IKK, prior to NF- κ B translocation (Hayden and Ghosh, 2012). Upon activation, neutral IKK becomes active IKK and degrades I κ B α initiating NF- κ B translocation. Active IKK gradually becomes inactive IKK, which then cycles

back to the neutral state over time (Behar and Hoffmann, 2013). We added two differential equations to describe this cycling of IKK (Equations 10 and 11). Then, we incorporated the two negative feedbacks discussed in our study. Upstream of IKK, MyD88-dependent ligands (LPS or IL-1 β) converge on another common kinase, IRAK1/4, which was shown to have auto-inhibitory negative feedback function reliant on aggregation (DeFelice et al., 2019). To integrate this important upstream negative feedback, we added IRAK1/4 activation and inactivation dynamics for each MyD88-dependent receptor (Equation 6–9). To minimize variables, we assumed that the activation and inactivation rates by different receptors are the same, and thus that IRAK1 kinetics depend only on the amount of each receptor in the active state. Since the inactivation rate varied by the amount of active IRAK, we made the inactivation term non-linear, where the inactivation rate is proportional to the squared concentration of active IRAK. Another important negative feedback originates downstream of NF- κ B. Other than I κ B α , previous works report many downstream genes, which inhibit nuclear NF- κ B in various ways (Renner and Schmitz, 2009). Among them, several inhibitors target upstream of IKK, where many negative feedbacks including A20, SOCS-1/3, and Trim30 α , repress the receptor activity and thereby hinder the activation of IKK. Hence, we added the expression of the downstream negative inhibitor (Equations 4 and 5) and adjusted the IKK activation term in Equation 10 to incorporate this effect. The Hill coefficient of 3 in this inhibition term includes the high cooperativity that arises in the complex interactions between upstream molecules. For example, for A20 to be fully active, it not only needs to be dimerized but also needs other adaptor proteins to inhibit the phosphorylation of IKK (Shembade et al., 2010). Additionally, IKK has multiple phosphorylation sites, which may require multiple inhibitor complexes to successfully repress the IKK activation (Delhase et al., 1999). Lastly, for the amount of activate ligand receptors, we normalized the dose range of ligand such that similar dose would activate similar number or ratio of receptors. For simplicity, we applied fast equilibrium approximation for the receptor dynamics, *i.e.*, at any given time the activity of receptor simply corresponds to the dose of ligand (Equation 12–14). All receptors investigated in our study require multimerization to be active (Kawasaki and Kawai, 2014; Wajant and Scheurich, 2011); hence, we used non-linear relationship between the dose and the active receptor. The system of equations for our model is listed below:

$$\frac{dN_n}{dt} = r_{Nim} * \frac{1 - N_n}{K_{lc} + 1} - r_{lim} * \frac{I * N_n}{K_{ln} + N_n} \quad (\text{Equation 1})$$

$$\frac{dl_m}{dt} = tr_l * \frac{N_n^4}{(K_N^4 + N_n^4)} - d_{lm} * l_m \quad (\text{Equation 2})$$

$$\frac{dl}{dt} = tl_l * l_m - a_{IKK} * IKK_a * (1 - N_n) * \frac{l}{K_{lc} + l} \quad (\text{Equation 3})$$

$$\frac{dA_m}{dt} = tr_A * \frac{N_n^4}{K_N^4 + N_n^4} - d_{Am} * A_m \quad (\text{Equation 4})$$

$$\frac{dA}{dt} = tl_A * A_m - d_A * A \quad (\text{Equation 5})$$

$$\frac{dIRAK_{LPS}}{dt} = a_{IRAK} * R_{LPS} * (1 - IRAK_{LPS} - IRAK_{iLPS} - IRAK_{iL1} - IRAK_{iIL1}) - d_{IRAK} * IRAK_{LPS}^2 \quad (\text{Equation 6})$$

$$\frac{dIRAK_{iLPS}}{dt} = d_{IRAK} * IRAK_{LPS}^2 - d_{IRAKi} * IRAK_{iLPS} \quad (\text{Equation 7})$$

$$\frac{dIRAK_{iL1}}{dt} = a_{IRAK} * R_{iL1} * (1 - IRAK_{LPS} - IRAK_{iLPS} - IRAK_{iL1} - IRAK_{iIL1}) - d_{IRAK} * IRAK_{iL1}^2 \quad (\text{Equation 8})$$

$$\frac{dIRAK_{iIL1}}{dt} = d_{IRAK} * IRAK_{iL1}^2 - d_{IRAKi} * IRAK_{iIL1} \quad (\text{Equation 9})$$

$$\frac{dIKK_a}{dt} = (1 - IKK_a - IKK_i) * a_R * \left(R_{TNF} * \frac{C^3}{C^3 + A^3} + IRAK_{LPS} * \frac{C^3}{C^3 + A^3} + IRAK_{IL1} * \frac{C^3}{C^3 + A^3} \right) - \mu * IKK_a^2 \quad (\text{Equation 10})$$

$$\frac{dIKK_i}{dt} = \mu * IKK_a^2 - \beta * IKK_i \quad (\text{Equation 11})$$

$$R_{TNF} = \frac{TNF^3}{TNF^3 + 1} \quad (\text{Equation 12})$$

$$R_{LPS} = \frac{LPS^3}{LPS^3 + 1} \quad (\text{Equation 13})$$

$$R_{IL1} = \frac{IL1^3}{IL1^3 + 1} \quad (\text{Equation 14})$$

Values for parameters

Even though our model consists of the two negative feedbacks and multiple receptors, we managed to reduce the number of parameters to twenty. Roughly half of these are related to NF- κ B and I κ B α dynamics. The other half describes the newly added mechanisms, which involve dynamics of IKK cycling and negative feedback regulations. Since our model is based on the minimal model from the previous publications, we adapted parameters from them to where applicable. For the newly added components, we assumed or fitted the parameters to the period of NF- κ B oscillation (\sim 2h). The list of parameters and their values are described in the table (Hoffmann et al., 2002; Krishna et al., 2006; Son et al., 2021; Tay et al., 2010).

Description	Parameter	Value	Unit	Reference
Importation rate of cytosolic NF- κ B into nucleus	r_{Nim}	11.3	$\mu\text{M} \cdot \text{h}^{-1}$	Hoffmann et al., 2002
Dissociation constant for I κ B α binding to NF- κ B in cytosol	K_{Ic}	3.5×10^{-2}	μM	Krishna et al., 2006
Importation rate of cytosolic I κ B α into nucleus	r_{Iim}	1.09	h^{-1}	Hoffmann et al., 2002
Dissociation constant for I κ B α binding to NF- κ B in nucleus	K_{In}	2.90×10^{-2}	μM	Krishna et al., 2006
Transcription rate of I κ B α mRNA	tr_I	59.5	$\mu\text{M} \cdot \text{h}^{-1}$	Hoffmann et al., 2002
Dissociation constant for nuclear NF- κ B inducing downstream transcription	K_N	0.6	μM	fitted
Degradation rate of I κ B α mRNA	d_{Im}	2.00	h^{-1}	Krishna et al., 2006
Translation rate of I κ B α	tl_I	14.4	h^{-1}	Hoffmann et al., 2002
Degradation rate of I κ B α by active IKK	a_{IKK}	126	$\mu\text{M}^{-1} \cdot \text{h}^{-1}$	Hoffmann et al., 2002
Transcription rate of downstream feedback mRNA	tr_A	5.0	$\mu\text{M} \cdot \text{h}^{-1}$	fitted
Degradation rate of downstream feedback mRNA	d_{Am}	1.0	h^{-1}	Tay et al., 2010 and Son et al., 2021
Translation rate of downstream feedback proteins	tl_A	15.0	h^{-1}	fitted
Degradation rate of downstream feedback proteins	d_A	0.25	h^{-1}	fitted
IRAK activation rate by active MyD88-dependent receptor	a_{IRAK}	252	h^{-1}	fitted
IRAK inactivation rate	d_{IRAK}	200	$\mu\text{M}^{-1} \cdot \text{h}^{-1}$	fitted
Rate for inactive IRAK to go back to neutral state	d_{IRAKi}	0.005	h^{-1}	fitted
Rate for either active TNFR or IRAK activating neutral IKK	a_R	4.00	h^{-1}	assumed
Dissociation constant for downstream feedback inhibiting IKK activation	C	8.0	$\mu\text{M}^{-1} \cdot \text{h}^{-1}$	fitted
Inactivation rate of active IKK	μ	28.3	$\mu\text{M}^{-1} \cdot \text{h}^{-1}$	fitted
Rate for inactive IKK going back to neutral state	β	0.2	h^{-1}	fitted

Running simulations

Computer simulations were performed using Python. The differential equations were integrated using *odeint* from *scipy.integrate* solver. To determine the basal stationary state of the network prior to stimulation, a short pulse of TNF- α was introduced at the beginning, then the dynamic of each component in the network was monitored up to 48 h after the pulse. After confirming the dynamics of all components became stationary, we stimulated the network with one of the first ligands (TNF- α , IL-1 β , or LPS), then replaced it with another ligand after 2 h. Simulated dynamics of different components were plotted using Bokeh visualization library.

To simulate the difference in the expression level of the downstream negative feedback, we adjusted the dissociation constant for the inhibition of IKK activation (parameter C). If we added the different downstream expression parameters for each ligand, it would dramatically increase the number of parameters necessary to describe the dynamics of downstream negative feedback. To simply model differential strength of IKK inhibition, we adjusted the dissociation constant for IKK inhibition. For LPS stimulation, the dissociation constant was reduced by four-fold, meaning the threshold for negative feedback molecules to inhibit the IKK activation is reduced by four-fold. This way we could still monitor the effect from the different downstream negative feedback strength, while minimizing the number of parameters.

Information theory analysis

For the information theory analysis, we employed the method and codes developed by Selimkhanov et al. (Selimkhanov et al., 2014). After obtaining the dynamics of NF- κ B translocation in each cell, the nuclear NF- κ B level at multiple time points were extracted and used as response (variable R) to evaluate the mutual information (variable I). Briefly, the mutual information is equal to the difference between the entropy of entire response (i.e., non-conditional entropy) from all samples and the sum of entropies from response in each sample (conditional entropy) (Shannon, 1948):

$$I(R; S) = H(R) - H(R|S)$$

where I indicates the mutual or transfer information and H indicates the entropy. Thus, I describes the reduction of uncertainty in 'guessing' which sample the response came from after observing the response. However, each sample may have different probability of happening. For example, in the case of this study, cells may be exposed a particular ligand sequence more frequently than other sequences. The conditional entropy can fluctuate depending the probability of each sample (or ligand sequence). However, it is still possible to evaluate the theoretical maximum information transfer possible through the given system. This is defined as channel capacity, C , and can be evaluated by finding a set of probabilities that would maximize the mutual information:

$$C(R; S) = \max_Q I(R; S) \begin{cases} \sum_i q_i = 1 \\ q_i \geq 0 \end{cases}$$

where C indicates the channel capacity, Q is a set of probabilities for m samples, $[q_1, q_2, \dots, q_m]$. Further details about the calculating entropies and how the mutual information was maximized can be found in the previous publication (Selimkhanov et al., 2014). In this study, the NF- κ B levels at multiple time points during each ligand interval in each sample were used as input (variable R) to calculate the channel capacity of NF- κ B network in distinguishing a particular ligand at each step (S1-4) or prior history of ligand.

QUANTIFICATION AND STATISTICAL ANALYSIS

Statistical analysis was performed using MATLAB for data from image analysis or R for data from qPCR measurements and RNA-seq. Data from images were analyzed using Bonferroni corrected Wilcoxon Rank Sum Test due to non-normality of distribution and are displayed as violin plots including all datapoints with mean highlighted and significance noted. qPCR data show mean +/- S.E.M. and significance determined using Benjamini-Hochberg adjusted two-tailed t -tests. n for each experiment, significance, and effect sizes are listed in figure legends.